National Laser Users' Facility and External Users' Programs

During FY04, 802 target shots were taken on OMEGA for external users' experiments, accounting for 51.5% of the total OMEGA shots produced this year. External users in FY04 included eight collaborative teams under the National Laser Users' Facility (NLUF) program as well as collaborations led by scientists from the Lawrence Livermore National Laboratory (LLNL), Los Alamos National Laboratory (LANL), Sandia National Laboratory (SNL), Naval Research Laboratory (NRL), and the Commissariat à l'Énergie Atomique (CEA) of France.

NLUF Program

FY04 was the second of a two-year period of performance for the nine NLUF projects approved for FY03–FY04 funding and OMEGA shot time. Eight of the nine NLUF campaigns received a total of 127 shots on OMEGA in FY04.

The Department of Energy (DOE) issued solicitations in FY04 for NLUF proposals for work to be carried out in FY05–FY06. DOE raised the available NLUF funding to $1,000,000 for FY04 proposals to accommodate the high level of interest in using OMEGA to carry out experiments of relevance to the National Nuclear Security Agency (NNSA) Stockpile Stewardship Program (SSP). NLUF participants use these funds to carry out experiments on OMEGA (including graduate student stipends, travel, supplies, etc.). The participants do not pay any portion of the OMEGA operating costs since these costs are funded directly by the DOE–LLE Cooperative Agreement.

A total of 16 NLUF proposals were submitted to DOE for consideration for FY05–FY06 support and OMEGA shot allocation. An independent DOE Technical Evaluation Panel comprised of Dr. Tina Back (LLNL), Dr. Robert Turner (LLNL), Dr. Steven Batha (LANL), Dr. Ramon Leeper (SNL), and Prof. Ani Aprahamian (University of Notre Dame) reviewed the proposals on 15 June 2004 and recommended that up to 8 of the 16 proposals receive DOE funding and 7 of the 8 teams be approved for shot time on OMEGA in FY05–FY06. Table 100.V lists the successful proposals.

FY04 NLUF Experiments

Programs carried out in FY04 by eight groups of NLUF participants included the following OMEGA experiments:

Optical Mixing Controlled Simulated Scattering Instabilities (OMC SSI): Generating Electron Plasma Waves and Ion-Acoustic Waves to Suppress Backscattering Instabilities
Principal Investigator: B. B. Afeyan (Polymath Research, Inc.)

The goal of this experiment is to examine the suppression of backscattering instabilities by the externally controlled generation of ion-acoustic-wave (IAW) or electron-plasma-wave (EPW) turbulence. The experiments consist of using optical mixing techniques to generate resonant waves in flowing plasmas created by the explosion of target foils by the OMEGA laser.

During FY04, experiments were conducted in which two blue beams as well as a blue beam and a green beam were crossed. Nineteen target shots were taken for this experiment in September 2004 using three new high-intensity-interaction-beam phase plates [known as continuous phase plates (CPP's)] designed by Sham Dixit of LLNL. They provided a near-10^{15} W/cm^2 interaction-beam intensity for 1 ns with 500 J of blue-beam energy. The same design was used for a green-beam CPP. In addition, a polarization rotator was fielded on the probe beams of the pump–probe experiments so as to discriminate against processes that do not involve the ponderomotive force generated by the beating of the pump and probe beams directly. The results of these experiments will be described in future publications. The principal conclusion of this six-year-long effort with crossing blue–blue and blue–green beams on OMEGA is that OMC SSI via IAW's is a significant potential tool for the suppression of stimulated Raman backscattering SRBS in high-intensity laser–plasma interaction.

Studies of Ion-Acoustic Waves (IAW's) Under Direct-Drive NIF Conditions

Principal Investigator: H. Baldis (University of California, Davis)

Stimulated Brillouin scattering (SBS) is of concern to laser fusion using the indirect-drive or direct-drive approach. Generally, it is believed that SBS is only a minor effect for direct-drive inertial confinement implosion experiments, particularly those currently conducted on OMEGA. However, scattered-light spectra collected in these implosion experiments show changes from the incident spectra that can arise only from nonlinear effects such as SBS. To extrapolate the present results to future larger direct-drive laser fusion experiments, it is necessary to understand the details of the present observations.

To gain better insight into the underlying processes, a series of OMEGA shots was dedicated to measuring SBS in planar geometry with 11 low-intensity beams producing a plasma and one or two interaction beams at oblique incidence. One of the interaction beams was beam 30 for which there is a full-aperture backscattering station on OMEGA (FABS30). Beam 30 was incident at ~42° to the target normal. The target normal was pointed between the two interaction beams (beams 15 and 30). Thus the specular reflection from beam 15 was also collected by FABS30. In addition, one expects SBS side-scattering to be enhanced in the specular direction due to possible self-seeding of SBS by the specular reflection at the turning point of beam 15. There could be an additional contribution to the light collected by FABS30 from a synergistic interaction between beams 30 and 15 if they are present simultaneously.

All of these conditions are also encountered in spherical implosion experiments. In spherical implosion experiments, however, many different angles of incidence are present simultaneously and may contribute differently depending on the time during the laser pulse. This makes it difficult to unravel the subtleties of the interaction processes, hence the choice of the planar geometry for this series of experiments.

Table 100.V: FY05–FY06 Proposals.

Principal Investigator	Affiliation	Proposal Title
J. Asay	Washington State University	Isentropic Compression Experiments for Measuring EOS on OMEGA
H. Baldis	University of California, Davis	Laser–Plasma Interactions in High-Energy-Density Plasmas
R.P. Drake	University of Michigan	Experimental Astrophysics on the OMEGA Laser
R. Falcone	University of California, Berkeley	NLUF Proposal: Plasmon Density of States in Dense Matter
R. Jeanloz	University of California, Berkeley	Recreating Planetary Core Conditions on OMEGA
P. Hartigan	Rice University	Astrophysical Jets and HED Laboratory Astrophysics
R. Mancini	University of Nevada, Reno	Three-Dimensional Study of the Spatial Structure of Direct-Drive Implosion Cores on OMEGA
R. Petrasso and C. K. Li	Massachusetts Institute of Technology	Implosion Dynamics and Symmetry from Proton Imaging, Spectrometry, and Temporal Measurements

A typical purely sidescattered signal is shown in Fig. 100.59 for a 1-ns square pulse interaction beam at ~2×10^{14} W/cm^2 in beam 15 (beam 30 was not fired). Also shown in Fig. 100.59 for comparison is the input laser spectrum. We note that the basic features of this time-resolved spectrum are the same as for spherical implosions. The initial rapid blue shift reflects the increasing plasma column traversed by the interaction beam as the plasma is formed. This is followed by a return toward zero overall spectral shift as the plasma column becomes stationary. The important difference between the incident and reflected spectra is in the shape of the spectrum late in time, which is narrower with a peak on the red part of the spectrum, compared to the incident spectrum shown as reference on the right side of Fig. 100.59.

Experimental Astrophysics on the OMEGA Laser

Principal Investigator: R. P. Drake (University of Michigan)

This NLUF project is led by the University of Michigan and involves collaborators from Lawrence Livermore National Laboratory; the Laboratory for Laser Energetics; the Universities of Arizona, Chicago, Princeton, and Stony Brook; as well as École Polytechnique and CEA from France. It uses OMEGA to study processes that are relevant to astrophysics, with a specific focus on the unstable nonlinear hydrodynamics that occurs when stars explode and on radiative shocks that occur during stellar explosions and in many other contexts. The experiments to study nonlinear hydrodynamics involved continuing examination of the role of initial conditions on the long-term nonlinear structure that develops after a blast wave encounters an interface. Data were obtained with a controlled variation of initial conditions and also to assess preheat levels. The experiments to study radiative shocks involved measurements of the change in shock velocity and structure with drive conditions and work to apply an improved diagnostic (a backlit pinhole) to obtain higher-resolution data.

Figure 100.60 shows a radiographic image from the radiative shock experiments, obtained using an area backlighter at 13.5 ns after the drive beams are fired. The grid and a fiducial feature establishing an absolute location are evident in the lower part of Fig. 100.60. The wall of the tube can be seen near the upper edge. The shock front is curved, and there are indi-

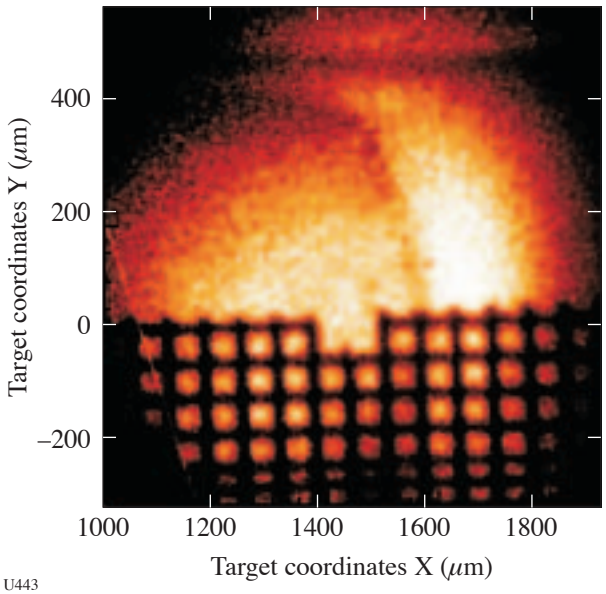

Figure 100.60
A radiographic image of collapsed radiative shock. This image is from an experiment with a polyimide drive disk attached to a polyimide tube of 912-μm inner diameter, irradiated (with SSD) at 9.3×10^{14} W/cm^2 onto a 720-μm laser spot. The illumination was by x rays from Ti produced by overlapping six laser beams.

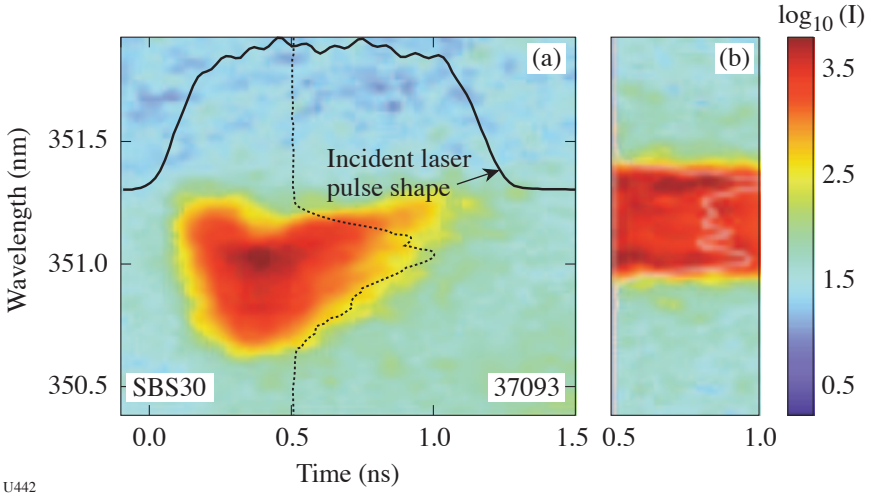

Figure 100.59
Stimulated Brillouin side scattering (a) from a planar plasma for an interaction beam at oblique (~42°) incidence at ~2×10^{14} W/cm^2. The plasma was simultaneously formed by 11 low-intensity laser beams. The incident laser pulse shape is shown as the dark line above the spectrum. A short but representative time slice of the incident laser spectrum is shown in (b). The vertical lineout through the spectra is also shown for both incident and reflected spectra.

cations of a trailing layer of dense xenon along the wall of the tube. The velocity and position of the center of the shock are within 10% of the values obtained from relevant 1-D simulations. The region of highest opacity is narrow, being 45 μm thick in this case. The layer of xenon produced by a nonradiative shock would be 140 to 220 μm thick at this location (depending on the exact equation of state). Thus, it appears that the density has increased another factor of 3 to 4 in consequence of radiative losses, reaching a total of 34 times the initial xenon density.

Recreating Planetary Core Conditions on OMEGA

Principal Investigator: R. Jeanloz (University of California, Berkeley)

During the past 18 months this team collected data on high-pressure H_2 and He fluids, combining diamond-anvil cells and laser-produced shocks (Fig. 100.61) to measure the first off-Hugoniot equation-of-state (EOS) data for both hydrogen (Figs. 100.62–100.64) and helium (Fig. 100.65) and to measure the highest-pressure EOS data ever for fluid helium. The

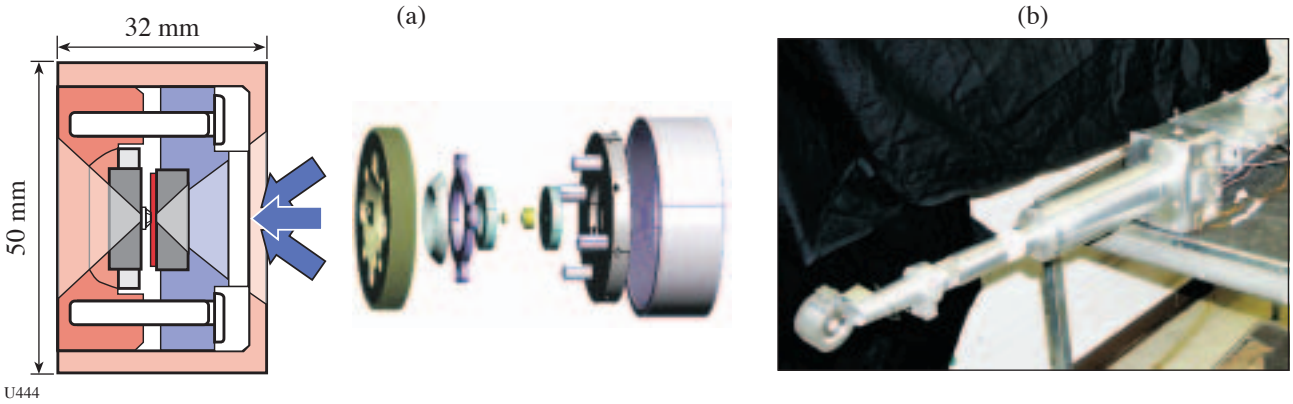

Figure 100.61
(a) Diamond-cell schematic and (b) photograph of target holder with diamond cell.

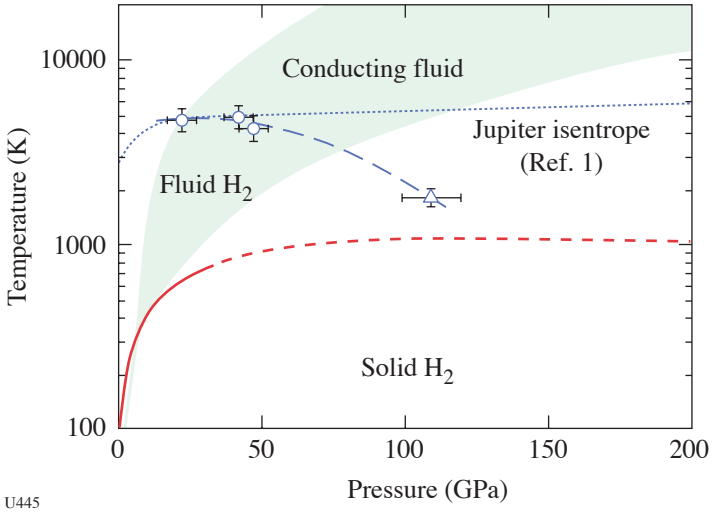

Figure 100.62
Phase diagram of fluid hydrogen, with results from laser-shock measurements on precompressed samples (circles with error bars) and reverberating-shock experiments (triangle with error bar) constraining the onset of conducting behavior with increasing pressure and temperature (dashed curve). The solid line (dashed where extrapolated beyond the pressure range of experiments) represents the determination of the melting curve of hydrogen, and the green area is the envelope of Hugoniot curves spanning the range from cryogenic hydrogen to hydrogen initially at 5 GPa

transformation of high-pressure helium from an insulator to an electronic conductor was observed [as documented by optical properties (Fig. 100.66)], and it was discovered that there is a correlation between the transition from insulating to conducting fluid phases of hydrogen and the proposed maximum in the melt curve.

A summary of how the new equation-of-state, reflectance, and temperature data impact our fundamental understanding of hydrogen is shown in Fig. 100.62. The open symbols show where, in T-P space, hydrogen is becoming electrically conducting, ~10^{19}e$^-$/cc; the conductivity saturates at slightly high pressure–temperature conditions, suggesting carrier concen-

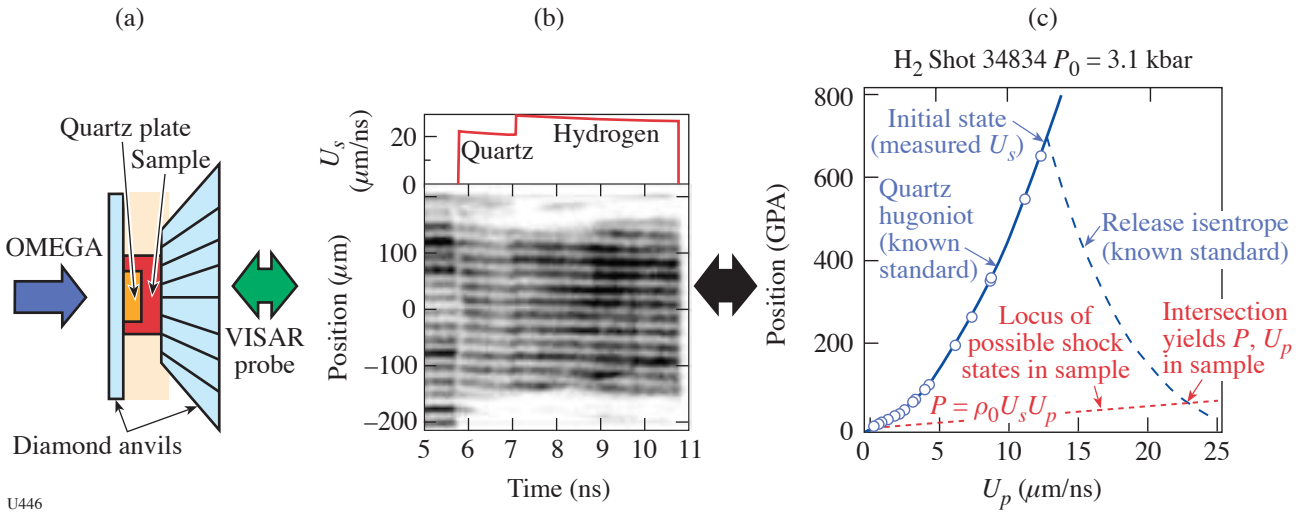

Figure 100.63
(a) Sketch of precompressed target, (b) sample VISAR record from precompressed H_2, and (c) example calculation for extracting pressure–density data. The beauty of this technique is that we observe the shock velocity in the quartz and the He or H_2 almost instantaneously, thus reducing much systematic and random uncertainties.

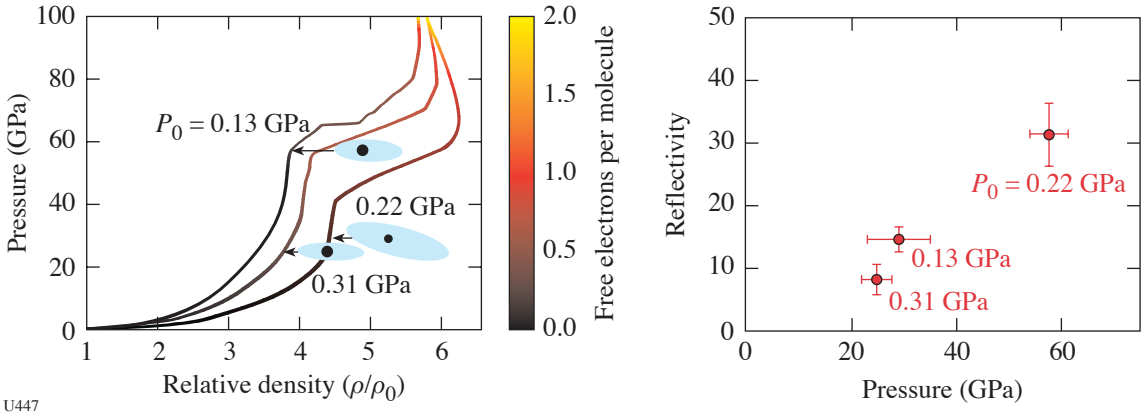

Figure 100.64
Measurements of shock density and optical reflectivity (532 nm) versus pressure for precompressed H_2.

trations near $10^{23}e^{-}$/cc. The line connecting the open symbols is very close to the theoretically predicted plasma phase transition, which is interesting, since in materials (such as carbon) that have a first-order liquid–liquid transition there is a maximum in the melt curve, as appears to be the case for hydrogen. Finally, note that this line also points to the single solid-state static experiment where conductivity is thought to be turning, or as evidenced by optical absorption above 310 GPa at 300 K. Each of these observations by itself is a notable result; all three represent a significant discovery.

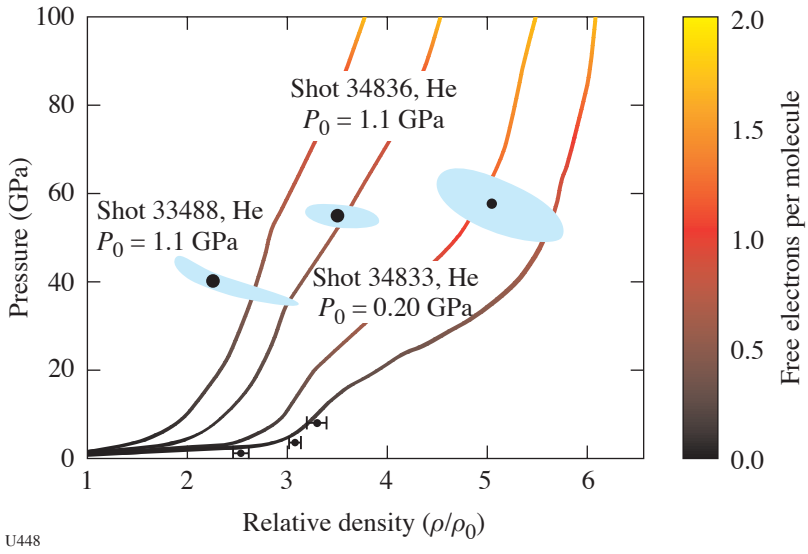

Figure 100.65
Pressure versus density shock-wave data for precompressed helium.

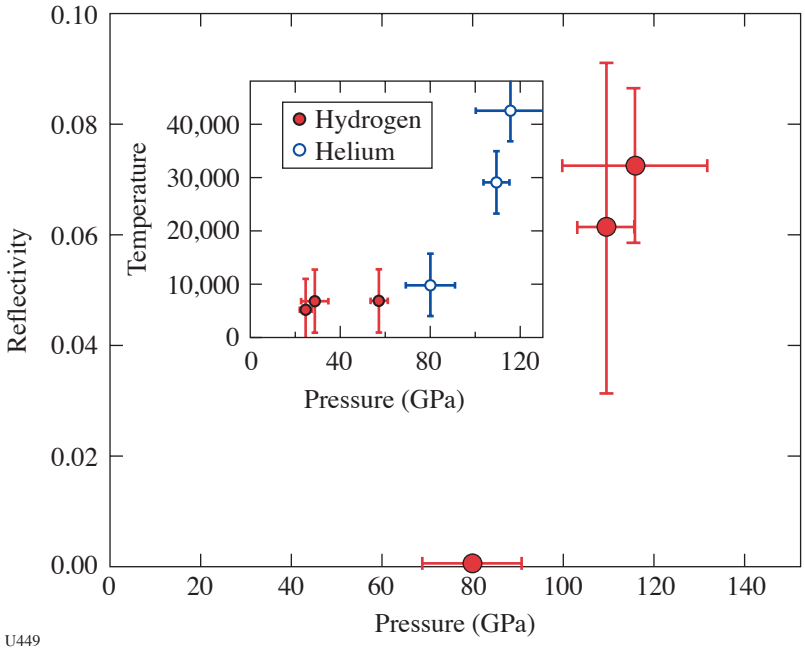

Figure 100.66
Shock reflectance at 532 nm as a function of shock pressure for He, with the inset showing the measured temperatures versus shock pressure for both He and H_2 data summarized in Figs. 100.64 and 100.65.

Experimental and Modeling Studies of 2-D Core Gradients in OMEGA Implosions

Principal Investigator: R. C. Mancini (University of Nevada, Reno)

During FY04, time-resolved (gated, Δt = 50 ps) x-ray images of argon-doped implosion cores were recorded in OMEGA indirect-drive shots, based on line emission from He_β, Ly_α, and Ly_β line transitions in He- and H-like argon ions, respectively. Images were obtained simultaneously along two quasi-orthogonal directions [TIM2 and TIM3 line of sight (LOS)] with two Multi-Monochromatic Imager (MMI-3) instruments that record on framing cameras. Analysis of these image data permits the extraction of time-resolved information on the spatial distribution of temperature, density, and mixing in the implosion core. In turn, these results can be compared with a previous analysis done using time-integrated image data.

Figure 100.67 shows simultaneous He_β- and Ly_β-based x-ray-gated images of the implosion core recorded in OMEGA indirect-drive shot 36980 along the TIM2 LOS. These images are integrated over a time interval of 50 ps, close to the peak of x-ray emission. By implementing a generalized Abel inversion procedure, spatial distributions of line emissivity can be extracted from the data on several core slices perpendicular to the hohlraum axis and characterized by a coordinate along this axis. Analysis of these emissivity maps can be performed via a multi-objective search and reconstruction method driven by a genetic algorithm, and by an independent analytic method where temperature is extracted from emissivity ratio maps and density is subsequently determined from analysis of He_β and Ly_β emissivity maps. Figure 100.67 displays results for electron temperature and density radial distributions in a core slice through the hohlraum midplane. Additional information on spatial mixing profiles can also be obtained by looking at differences between relative intensity distributions in the data and those predicted by spectral modeling. These differences can be related to the amount of plastic mixed into the deuterium fuel and play an important role in the determination of the density profile. The temperature profile is relatively insensitive to this effect. Figure 100.67 displays this information in terms of γ, which is defined as the local ratio of plastic to fuel densities.

Work is in progress to include quantitative data from Ly_α images and to compare analysis results obtained along quasi-orthogonal LOS.

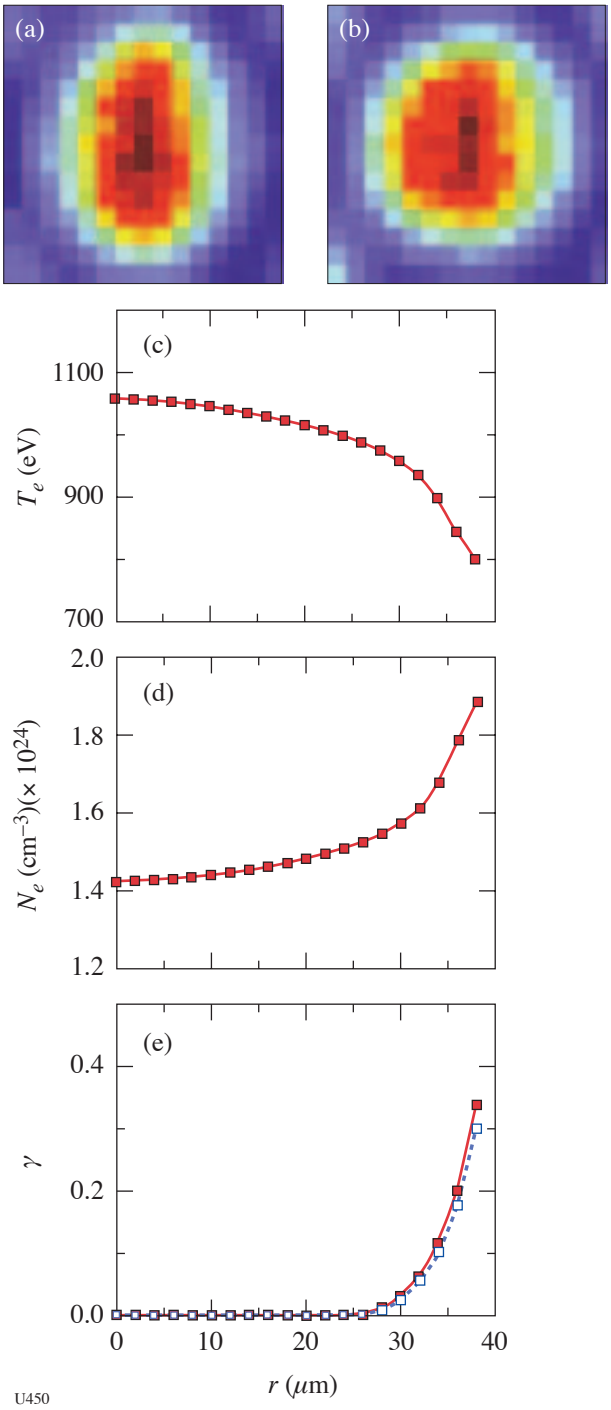

Figure 100.67
Simultaneous, time-resolved (gated, Δt = 50 ps) x-ray images based on argon He_β (a) and Ly_β (b) line emission from OMEGA indirect-drive shot 36980. The hohlraum axis is along the horizontal direction. Radial spatial distribution in the core's midplane (perpendicular to the hohlraum axis) of electron temperature (c) and density (d), and mixing of plastic into the fuel (e). Analysis assumes an isobaric core.

OMEGA Laser Studies of the Interaction of Supernova Blast Waves with Interstellar Clouds

Principal Investigator: C. F. McKee (University of California, Berkeley)

In the NLUF Astro experiment a planar shock is driven by the OMEGA laser inside a cylindrical shock tube. The shock passes by a sphere that is more dense than the surrounding material (by about a factor of 9). The sphere material is "crushed" and set in motion; it rolls up in a classical Kelvin–Helmholz instability, then transitions to a fully 3-D flow through a Widnall instability. This experiment has been a pioneer in using backlit pinhole technology, and considerable efforts were made to make this technique work reliably (e.g., using tilted pinhole substrates, "destroyer beams," and target alignment using small corner reticles). By November 2003 the images could be obtained both reliably and with good signal-to-noise quality. Shots on 20 November were aimed at studying the shocked sphere material at late times (>60 ns after the start of the experiment), something that had never been done before. Experimental images (Fig. 100.68) showed sphere material being extensively shredded at these times, and by 80 ns the sphere material had reached the detectability limits for the very sensitive backlit pinhole technique, suggesting that the material is in a turbulent state by this time.

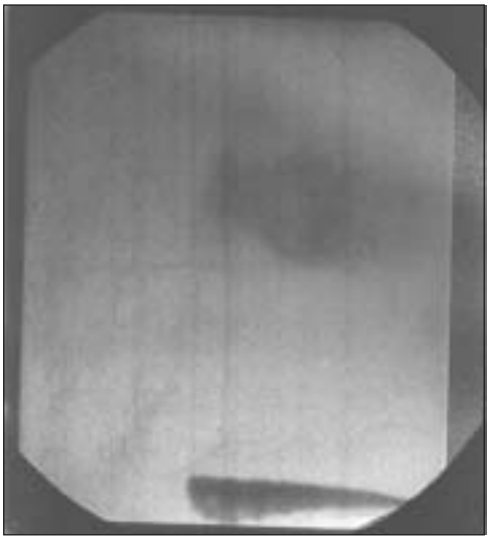

U451

Figure 100.68

Shocked sphere material 60 ns after the start of the experiment. Most of the sphere material makes up the bell-shaped object in the upper half of the image and has a volume more than 10 times larger than the original sphere (original sphere diameter 120 μm). Even with the high signal-to-noise ratio of the backlit pinhole technique, the sphere material is by this time quite diffuse; by 80 ns, it is no longer detectable. (The object in the lower half is a gold grid used as a spatial fiducial; one side of the image is approximately 1150 μm.)

The NLUF Astro experiment was awarded 15 shots (one and a half shot-days) on OMEGA during FY2004. One half-day of shots was carried out successfully on 20 November, but a full day of shots planned for 15 April could not be taken since other targets were given higher priority at LLNL's target fabrication facility.

Time Evolution of Capsule ρR and Proton Emission Imaging of Core Structure

Principal Investigators: R. D. Petrasso and C. K. Li (Plasma Science and Fusion Center, MIT)

During FY04 penumbral proton imaging was used to study the spatial distributions of D-D and D-^{3}He reactions in imploded D^{3}He-filled capsules on OMEGA. The imaging was performed with multiple cameras in which the recorder consists of stacked sheets of CR-39 nuclear track detector separated by ranging filters that result in the efficient detection of 14.7-MeV D^{3}He protons on one sheet and 3-MeV DD protons on another. The raw images were processed in two ways.

One approach was to assume that the emission distribution is spherical and to reconstruct a radial burn profile to study how the size of the burn region varies with capsule type and laser-illumination parameters. Figure 100.69 shows some data com-

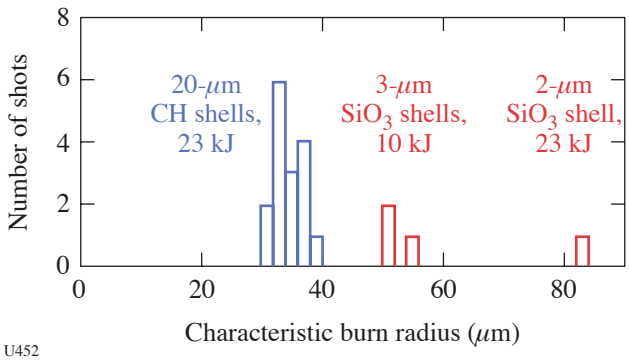

U452

Figure 100.69

The sizes of the D^{3}He burn regions in different types of implosions of D^{3}He-filled capsules (all capsules have 18-atm gas fills, and all laser pulses utilized SG3 phase plates). The burn profiles are nearly Gaussian, and the size is characterized by the radius at which the emissivity is down from the central value by 1/*e*. The thicker-CH-shell capsules implode with a higher convergence ratio than the thinner-SiO_2-shell capsules, resulting in smaller burn radii. The data point at 82 μm was obtained from an implosion with 23 kJ of incident laser energy, while the other SiO_2 data points had approximately 10 kJ of incident laser energy.

paring capsules with thin glass shells to capsules with thick CH shells. The thin-glass capsules clearly have a larger burn region and indicate less radial convergence at burn time.

The other approach was to reconstruct two-dimensional (2-D) images of the surface brightness of the capsule. There are now three cameras on OMEGA that can be used to image capsules from three orthogonal directions simultaneously for symmetry studies. Data from each are then used to reconstruct a 2-D map of surface brightness, and the three separate images provide information about three-dimensional (3-D) burn asymmetries. To study the relationship between illumination asymmetry and burn asymmetry, an experiment was performed recently with laser drive containing intentional P2 asymmetry. Laser intensity was reduced at the two poles of a symmetry axis, with the result that the capsule imploded with a prolate ("sausage"-shaped) asymmetry. Figure 100.70 shows the resultant burn asymmetry, measured with three orthogonally oriented proton-emission imaging cameras; one camera viewed the end of the sausage while the other two viewed the sides. A substantial elongation of the emission region is seen, with a ratio of about 3:1 between the long and short axes. The direction of the elongation is coincident with the axis of the illumination asymmetry. In addition, the data suggest that the emission is peaked at the two ends of the region, resulting in a "dumbbell"-like shape.

FY04 LLNL OMEGA Experimental Program

Lawrence Livermore National Laboratory (LLNL) conducted 431 target shots on OMEGA in FY04. Approximately half of the shots were for the High-Energy-Density Science (HEDS) Program, and the other half were for inertial confinement fusion (ICF) experiments. The ICF experiments are summarized as follows:

A campaign was initiated to examine the effect on a capsule of direct hydrodynamic pressure from the laser-heated fill gas in gas-filled hohlraums. Initial results (Fig. 100.71) showed that the backlit foamball surrogate gave good results at fill pressures above and below those ultimately desired. (This series will continue in FY05.) The interaction of a hohlraum gas fill during the hydrodynamically unstable deceleration phase was also measured; no substantial instability growth was observed, even from deliberately pre-roughened hohlraum surfaces (Fig. 100.72).

In the area of x-ray drive, experiments were continued with hohlraums constructed of a mixture of materials ("cocktails"), in an effort to optimize x-ray conversion efficiency, albedo, and also laser–plasma coupling. Currently, it is believed that the consistently lower-than-expected improvement in radiation temperature for cocktail hohlraums is due to low-Z contaminants. Additional experiments were carried out to assess

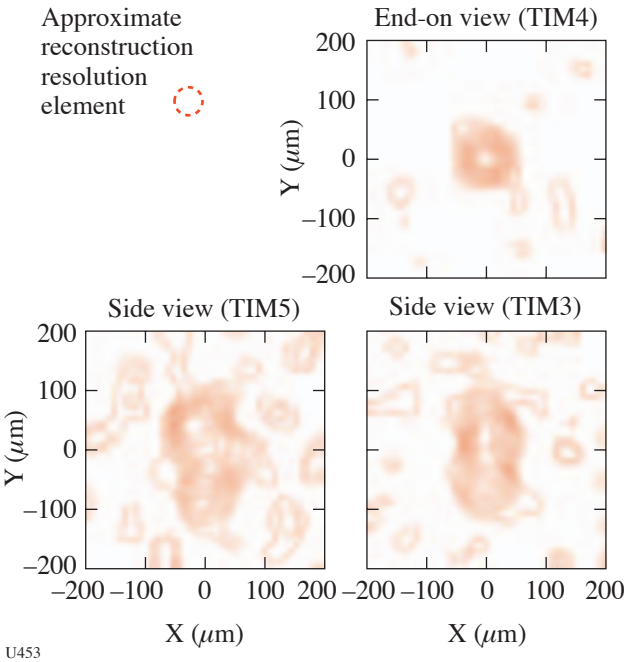

Figure 100.70
The first images of D^3He nuclear burn in an asymmetric implosion. These three contour plots show nearly orthogonal views of the fusion burn region in OMEGA implosions 35172 and 35173, recorded by three proton-emission cameras operating simultaneously (data from the two implosions are summed). The burn asymmetry had a prolate, or "sausage," shape, resulting from intentional asymmetry in the laser drive. The target capsules consisted of 20 atm of D^3He in 17-μm-thick CH shells, and the laser pulse delivered 17.5 kJ of on-target energy in a 1-ns square pulse. The laser intensity was lower than average in two directions 180° apart (on the TIM6–TIM4 axis), and the fusion burn is elongated in those directions. In the image reconstruction, bandwidth limitation for reducing noise resulted in an effective point-response function that is a Gaussian with ~20-μm radius; the dashed circle thus indicates the approximate reconstruction resolution.

the performance of lined or foam-filled hohlraums as alternates to the gas-filled National Ignition Facility (NIF) hohlraum point design. The early results are promising, showing radiation temperatures constant to within 5% between types of hohlraums and low levels of backscatter with smoothed beams at 5×10^{14} W/cm^2.

Laser–plasma–interaction studies were done on large-scale-length plasmas created by preheating large gas-filled targets with the main laser (Fig. 100.73). Various experiments, some

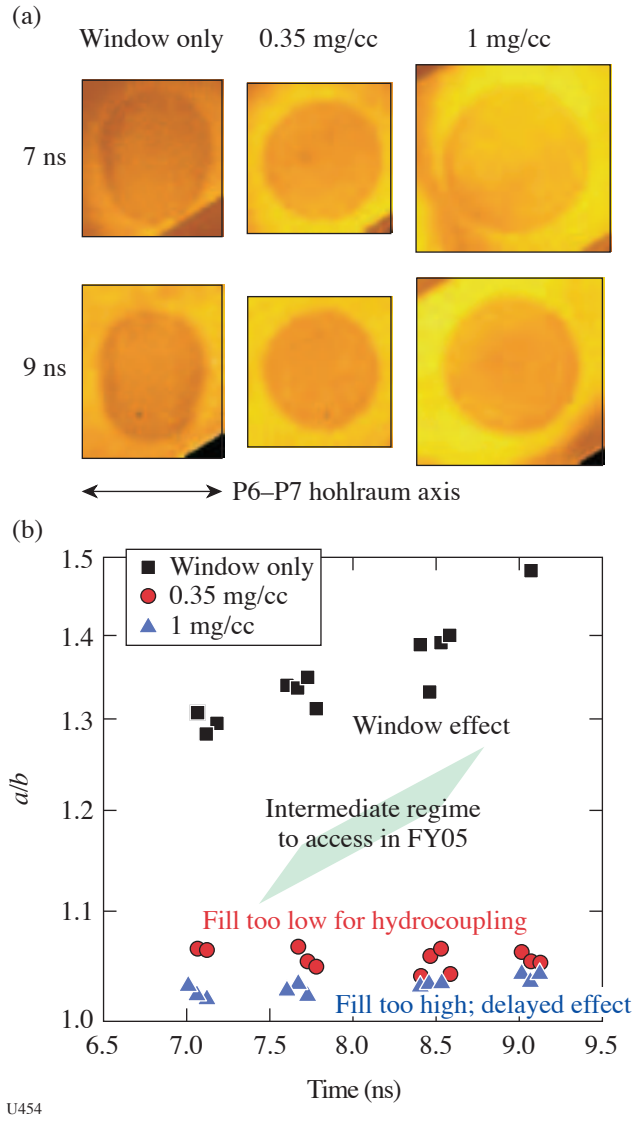

Figure 100.71
Backlit foam balls in CH (low-radiation)-gas–filled hohlraums are used to measure the gas-capsule hydrodynamic coupling. (a) Time-gated x-ray-backlit images of foam balls; (b) plot of foam-ball distortion versus time.

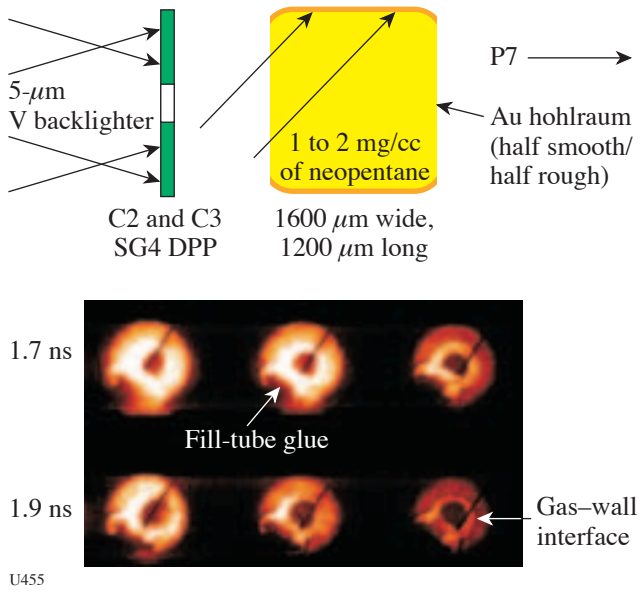

Figure 100.72
End-on view of an x-ray-backlit, gas-filled hohlraum shows wall motion and stagnation, with no signs of increased mix due to surface roughness.

using a 2ω or 4ω probe beam, were conducted to obtain data on stimulated Raman scattering (SRS), stimulated Brillouin scattering (SBS), and beam propagation (Fig. 100.74) as functions of beam-smoothing level. The results show reduced beam spray and backscatter by using increased smoothing on a 2ω probe beam. More crossing-beam power transfer experiments (a form of Brillouin scattering of special interest to the NIF) were performed as a function of polarization state (Fig. 100.75). Thomson scattering was used frequently to measure the electron temperature of these plasmas, while backscattered light (FABS) diagnostics monitored the amount of SBS or SRS. Still other experiments demonstrated the ability to measure the time-resolved spectrum of H- and He-like Ti (5-keV) x rays scattered by free electrons in a hot plasma; careful fits to the data yield temperature and density data (Fig. 100.76). Finally, a hohlraum experiment was conducted to quantify the amount of laser light that, at early times, is refracted from the hohlraum wall directly onto the implosion capsule.

Continued systematic improvements were made in using target-mounted pinholes to image implosion cores at moderately high (>7-keV) energies. Asymmetric core images were obtained at 87× magnification, demonstrating a method for measuring higher-order (up to 6, possibly 8) mode structure in the hohlraum drive (Fig. 100.77).

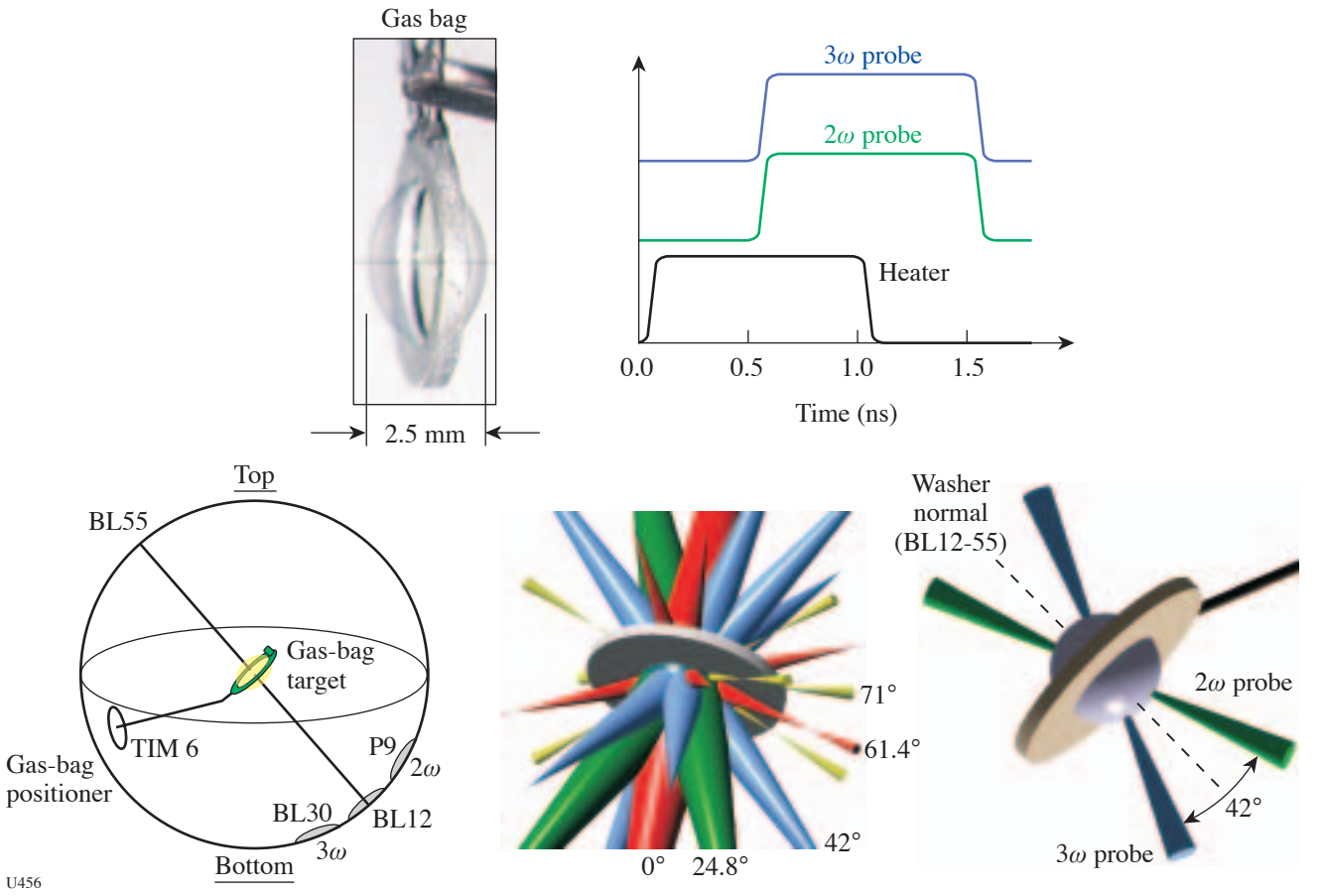

Figure 100.73
The LLNL laser–plasma interaction studies in FY04 used gas-bag targets to form large, well-characterized plasmas. The diagrams illustrate the target configuration used in these experiments.

New data were obtained on integrated hohlraum implosions with deliberately roughened capsules (Fig. 100.77). These experiments were performed with convergence ratios (CR's) of 15 and provide a stringent test for modeling hydrodynamic instabilities. These same experiments demonstrated a small difference in drive asymmetry—which resulted in a degradation in neutron yield—if the presence or absence of polarization rotators was not accounted for in the laser pointing.

Ablator material studies, focusing on the Rayleigh–Taylor growth factors, continued in FY04 on polyimide and brominated plastic (Fig. 100.78). The results confirmed greater-than-expected RM growth for the thinner samples, but as-predicted RT growth rates (Fig. 100.79). A new more-NIF-like, pulse-shaped, 2-D, symmetric, gas-filled halfraum experimental platform was designed for August 2004 shots. A first experiment was conducted to look at the effect of DT-fill tubes on an imploded capsule, using a deposited bump on the capsule as a surrogate for the fill tube.

Building on the work on hot hohlraums (see HEDS below), several implosion experiments were conducted using smaller-than-standard (3/4-size) hohlraums (Fig. 100.80). These represented the highest radiation-driven temperature implosions shot on laser facilities, reaching 275 to 285 eV, and producing symmetric cores. In some experiments DHe^3 supplied by LLE was used as the fuel; DHe^3 fusion proton yields and spectra were recorded and analyzed by MIT.

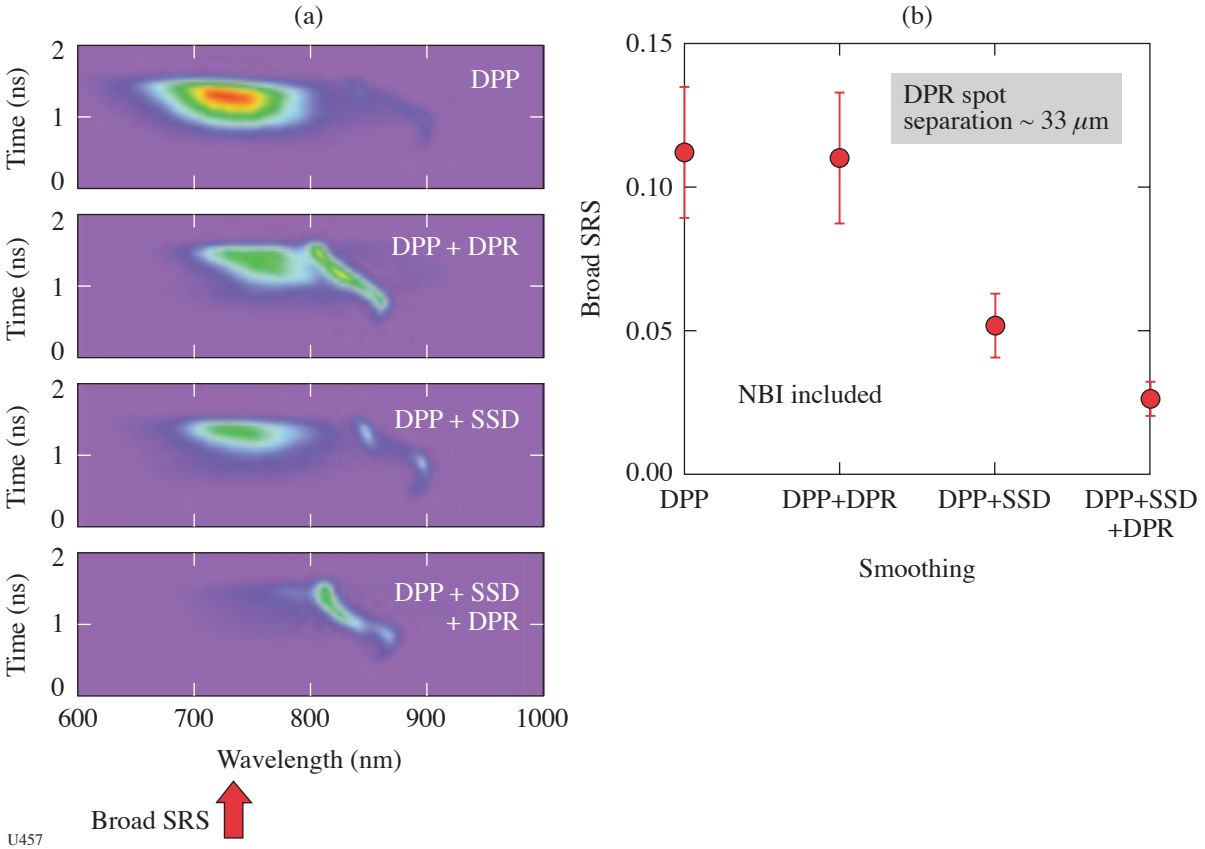

Figure 100.74
Laser-beam smoothing effectively reduces SRS in the low-density-plasma region. (a) Streaked SRS spectrum for four different laser irradiation beam-smoothing configurations. (b) Measured 2ω SRS scattered traction for the four different beam-smoothing configurations.

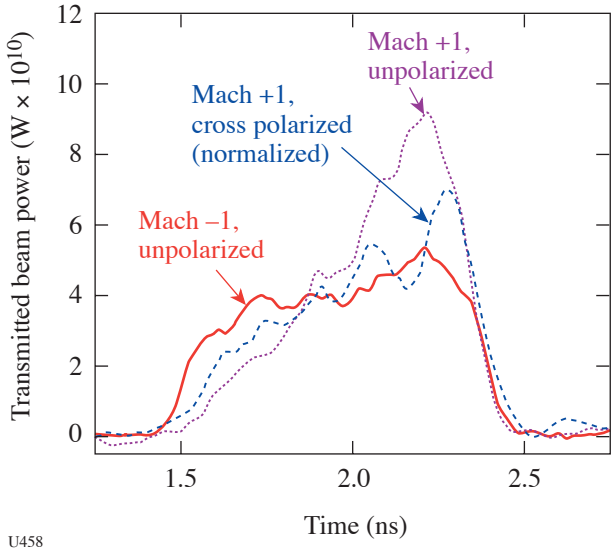

Figure 100.75
Crossed-beam experiments show energy transfer under the proper plasma flow conditions.

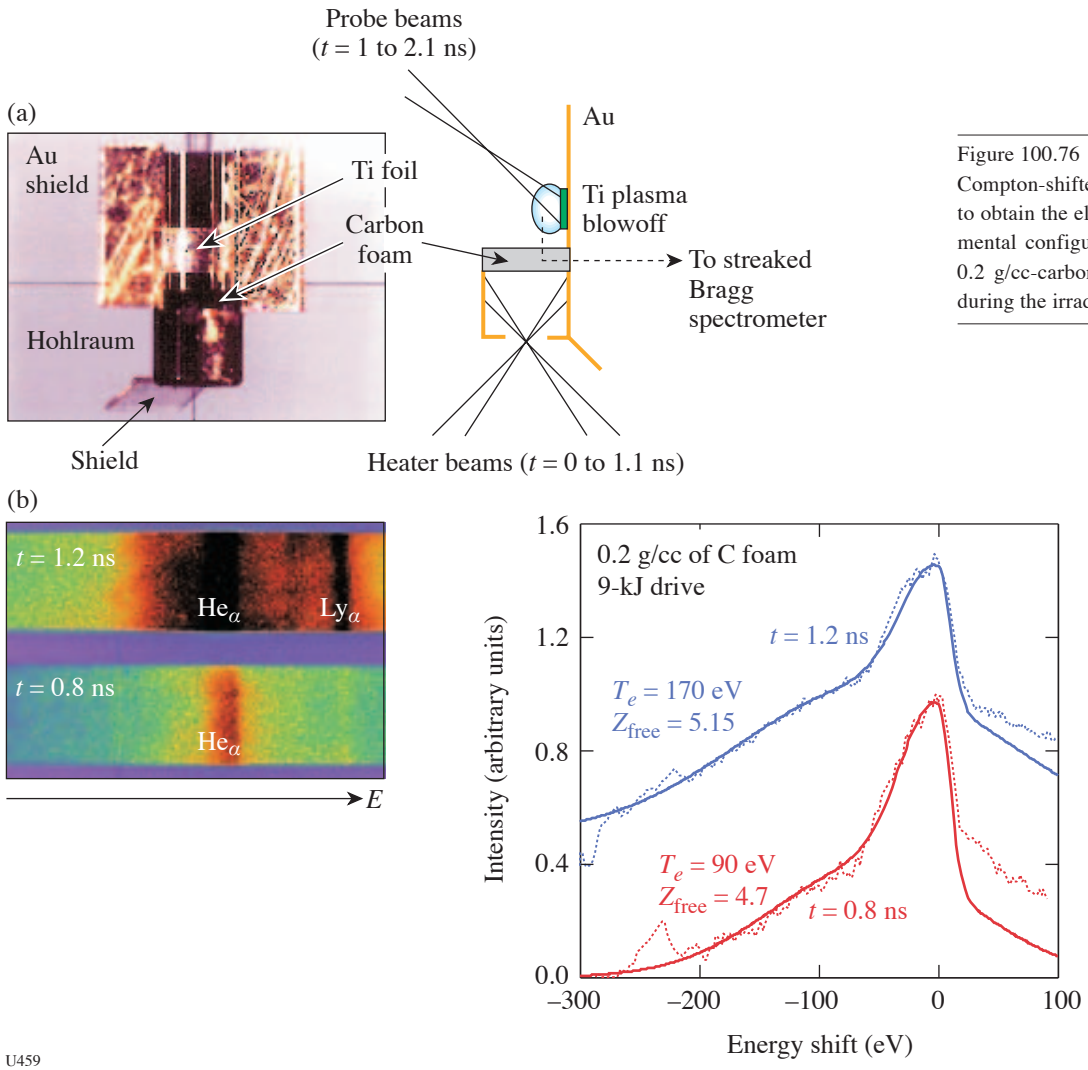

Figure 100.76
Compton-shifted scattered x rays are analyzed to obtain the electron temperature. (a) experimental configuration; (b) x-ray spectra from 0.2 g/cc-carbon foam at two different times during the irradiation.

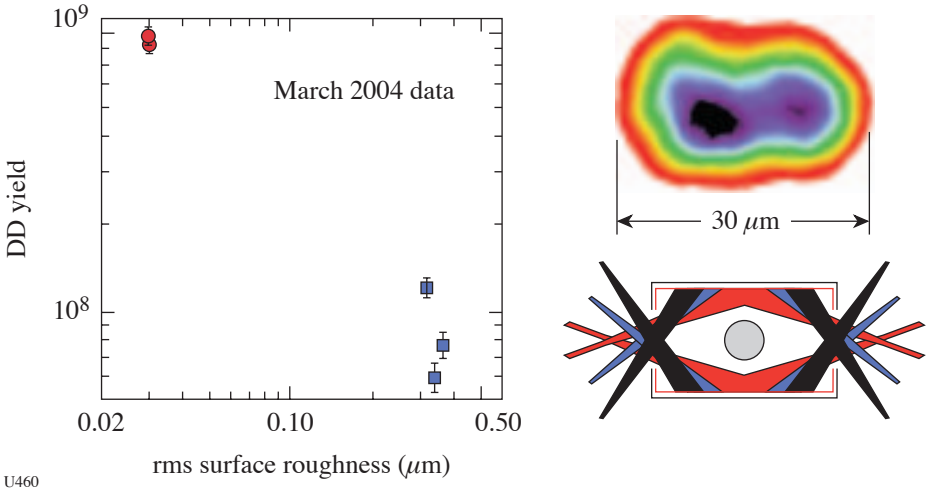

Figure 100.77
Neutron-yield degradation for implosions with a convergence ratio (CR) of 15 as a function of measured capsule-surface roughness. Also shown is a high-magnification x-ray image of an asymmetric imploded core, obtained at 8 keV.

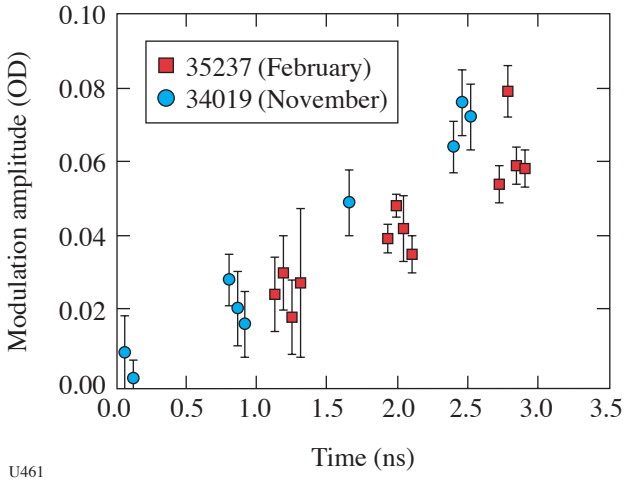

Figure 100.78
FY04 OMEGA polyimide Rayleigh–Taylor experiments measured the growth rate of hydrodynamic instabilities.

In collaboration with the University of Nevada, Reno (NLUF), multiple pinhole-imaged and spectrally dispersed data were obtained from indirectly driven, Ar-doped fuel implosions (Fig. 100.81).

Finally, several days of experiments were done in collaboration with LANL and LLE, using direct-drive, DT-filled targets, for the purpose of developing neutron diagnostics. These relatively high-yield shots have indicated that significant background will be present for any diagnostics or electronics that are neutron sensitive.

The other half of the LLNL shots were devoted to high-energy-density-science (HEDS)–relevant experiments. These are summarized as follows:

- Hot hohlraum experiments used hohlraums that were as small as possible to create as-high-as-possible radiation environments. Measurements were made on effective radiation temperature, high-energy ("suprathermal") x rays, and laser–target coupling.

- Equation-of-state (EOS) experiments continued on OMEGA in FY04. These involved VISAR measurements of shock propagation times in various materials. Other experiments focused on creating and using an adiabatic (shockless) drive (Fig. 100.82) to smoothly ramp up the pressure for EOS measurements of solid (not melted) materials (Fig. 100.83). Finally, experiments done in collaboration with an NLUF investigator used gases that were precompressed in a diamond anvil cell to explore equations of state relevant to the giant planets.

- OMEGA shots were also used to explore various options for obtaining x-ray point backlighters. It is expected this knowledge will be used on future OMEGA and NIF shots.

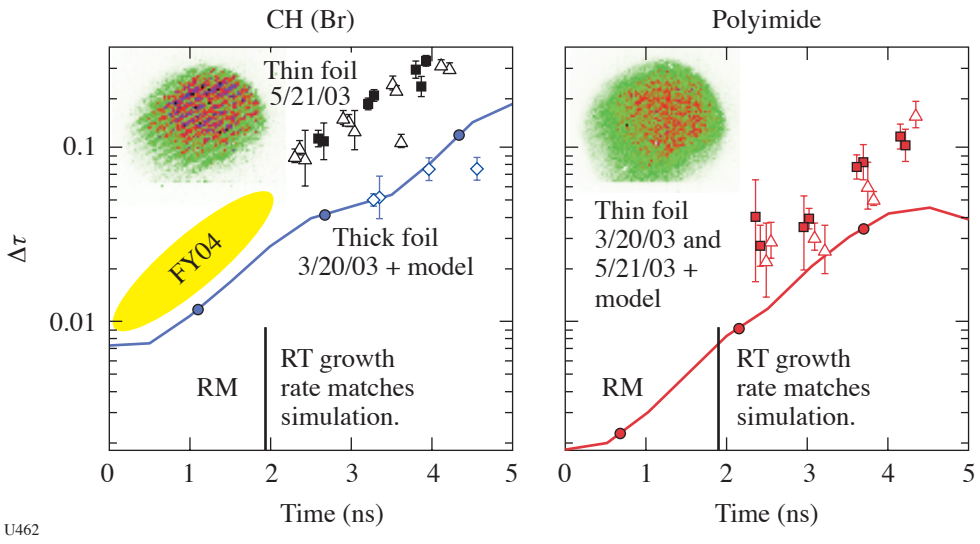

Figure 100.79
Plots of opacity versus time. The late-time data (~2 ns) show growth rates (slopes) consistent with the models, but a higher-than-expected growth during the early-time RM growth.

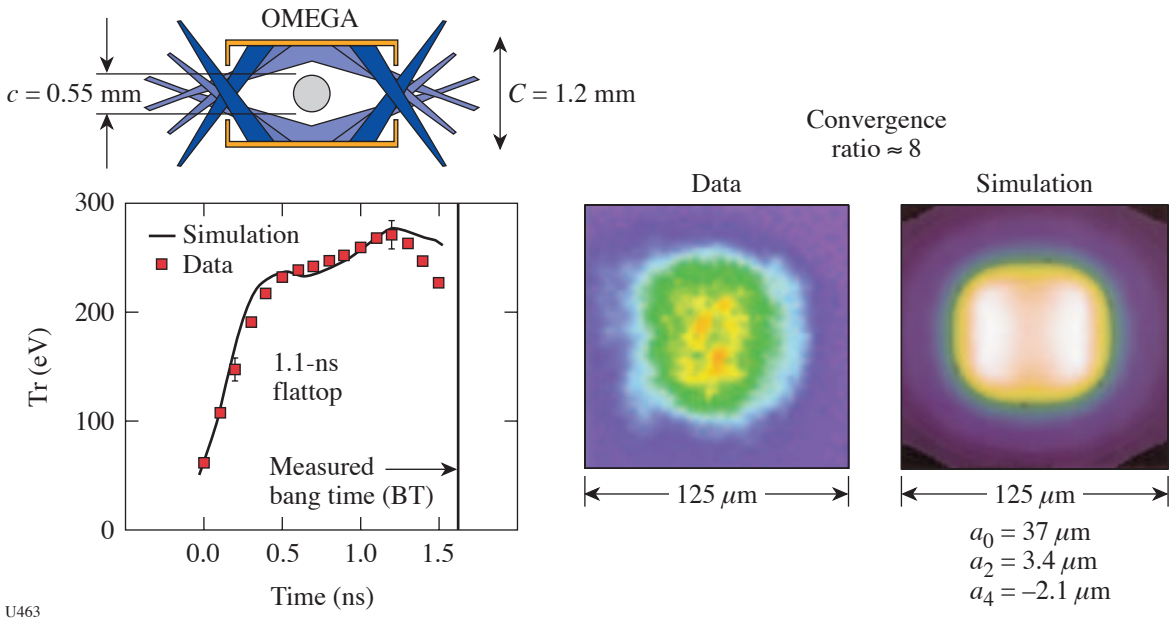

Figure 100.80
Low-convergence-ratio implosions in small, high-temperature hohlraums were used to confirm basic drive symmetry.

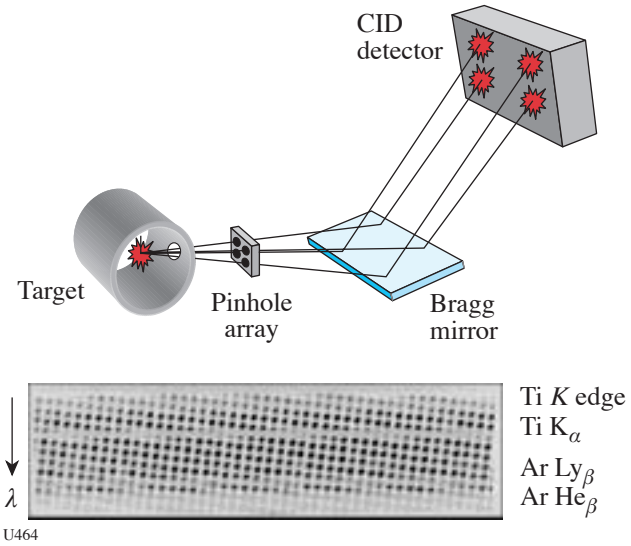

Figure 100.81
Geometry of spectrally dispersed imager used in NLUF experiments.

- A number of shots were devoted to studying alternative approaches to the standard indirect-drive concept of a simple hohlraum with a single-shell capsule. These included "dynamic hohlraums," where a high-Z gas is directly driven and compressed and its resulting x rays are used to drive a second, concentric implosion capsule; and "double shells," where the first driven shell collides with an inner shell, resulting in implosion velocity multiplication.
- The radiation flow campaign continued in FY04, focusing on x-ray propagation through low-density foams.
- A series of experiments were conducted to develop appropriate backlighter sources and detectors to measure the opacity of warm materials. The results of this campaign are expected to be used on experiments in FY05.
- LLNL continued a collaboration with LANL and AWE (United Kingdom) on the "Jets" experiments, looking at large-scale hydrodynamic features.
- Finally, shots onto gas-bag targets were conducted with various mid- to high-Z gases, in connection with developing x-ray sources (Fig. 100.84).

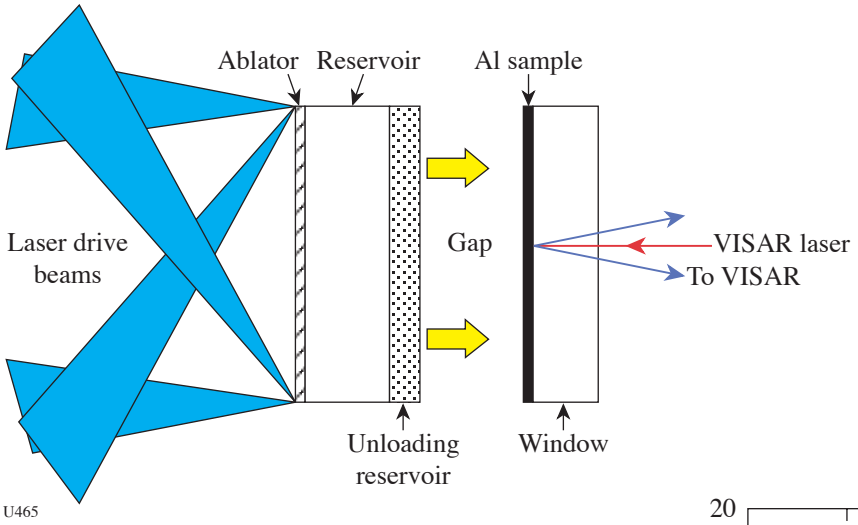

Figure 100.82
Experimental target setup used to produce smoothly increasing pressure drive for solid target physics.

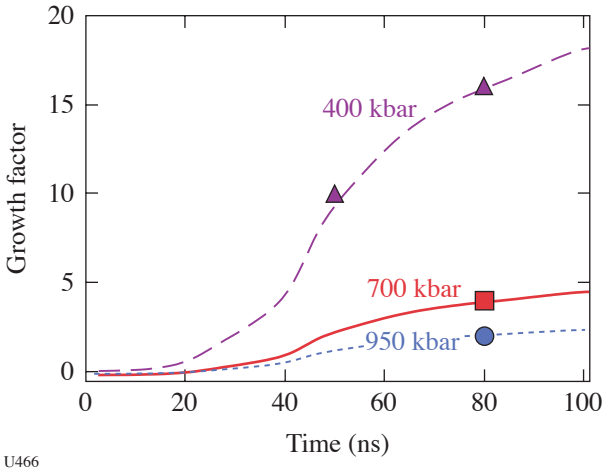

Figure 100.83
RT results for solid vanadium at three different pressures.

Targets:

Gas bag
Ar (0.1%) + CH_4 (99.9%)
p = 0.5 atm
Bag o.d.: 2.8 mm
Washer o.d.: 4.5 mm
Transmission: >30%

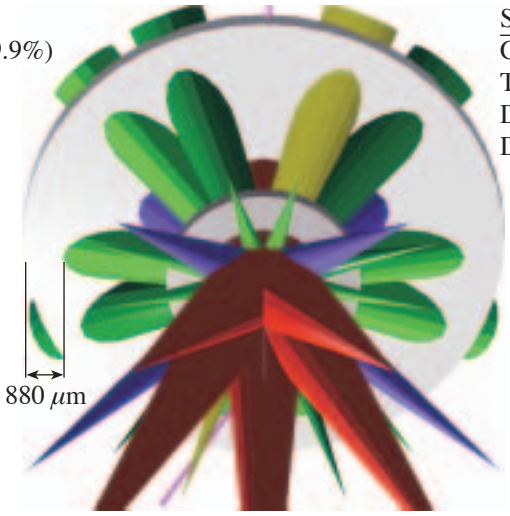

Stopper
CH foil
Thickness = 100 μm
Diameter = 11.5 mm
Distance to gas-bag center = 2 mm

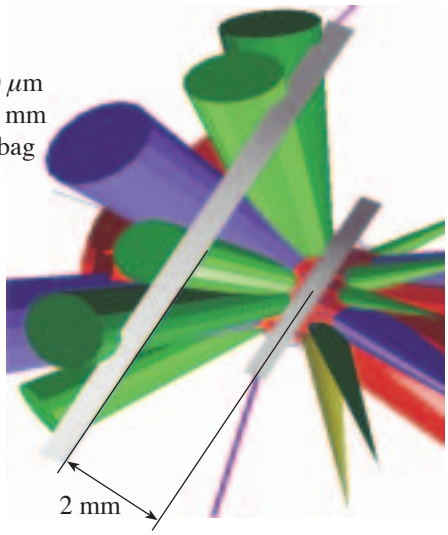

U467

Figure 100.84
Ar-doped gas-bag targets used to measure conversion efficiency to x rays.

FY04 LANL OMEGA Experimental Programs

Los Alamos National Laboratory (LANL) fielded a wide range of direct-drive-implosion experiments in both spherical and cylindrical geometries during FY04. The primary emphasis of these experiments was to measure mixing in convergent geometries to understand basic hydrodynamic behavior that will help validate our inertial confinement fusion (ICF) codes. Direct measurements of the stability of grainy Be were performed as part of the national effort to characterize ignition-capsule ablator materials. Collaborations with LLNL, LLE, and AWE are an important part of LANL's program on the OMEGA laser at LLE. The Astrophysical Jets experiment and the development of the Burn-History diagnostic were continued with these collaborating institutions. LANL also fielded its first experiments designed specifically as staging experiments for future execution on the NIF. LANL conducted a total of 168 target shots on OMEGA in FY04.

Time-Dependent Mix: The time-dependent evolution of mix was measured by imploding D_2-filled, plastic ICF capsules. These capsules include a 0.1-μm-thick layer of titanium-doped plastic on the inside surface as a spectroscopic probe of the mix. Specifically, mixing of titanium into the D_2 fuel greatly enhances the intensity of the hydrogen-like Ti α line relative to the helium-like Ti α line because high temperatures consistent with the imploded fuel core (>2.5 keV) are required to populate the upper state of the hydrogen-like Ti α line. Therefore, the time evolution of the intensity ratio of the hydrogen-like Ti α line to the helium-like Ti α line is a strong indicator of the amount and timing of shell material mixing into the hot-core region of the fuel. The experimentally measured intensity ratio was up to 50% larger than that predicted by the simulations. This intensity ratio suggests that more mix is occurring in the center of the fuel region than that predicted by the mix model used in the simulation. We cannot, however, be certain of this because the simulations also predict lower temperatures than those measured by neutron time-of-flight data. The cause of the temperature discrepancy is still an open question that is being investigated.

In addition to spectral line information from the titanium, time-resolved spectroscopic measurements, data from x-ray time-gated-imaging diagnostics and neutron-yield diagnostics were also used as indicators of the level and timing of mix occurring within the imploding capsules. The gated x-ray images showed that even at the earliest time possible, near when the reflected shock first reaches the ablator and about 150 ps before peak burn, the images are not limb-brightened, but instead have a flat profile that later becomes centrally peaked. This profile indicates substantial mix at a time when other experiments have suggested little and backs up the observations in the intensity ratio of the α lines. Unfortunately, only a few images were obtained at times of interest near the burn with the x-ray framing cameras. The images showed indications useful for unique timing in future experiments (such as the outward expansion of the shock after peak burn, faint interference by gamma rays at peak burn, and the sudden brightening when the reflected shock first reaches the pusher layer).

Time-gated images (Fig. 100.85) show the full time history of the implosion with an interstrip time of 700 ps. The first strip shows the initial capsule size, the second strip shows the capsule imploding, the third strip shows the effect of the neutron emission at the implosion time, and the fourth strip shows an outgoing shock after the implosion.

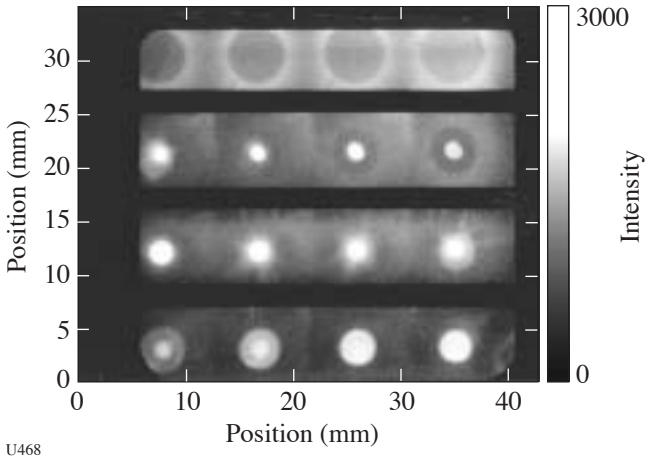

Figure 100.85
Time-gated x-ray images of a single capsule experiment showing both the implosion and explosion phases. Time runs from right to left and top to bottom.

Double-Shell Implosions: Imploding double-shell targets may provide an alternative, noncryogenic path to ignition on the NIF. Experiments are being pursued on OMEGA to understand the hydrodynamics of these implosions and the possibility of scaling to NIF designs. One line of inquiry this year measured the effect of foam structure on neutron yield. Carbon resorcinol foam [$C_6H_6O_2$], with cell sizes of a few nanometers, was used instead of the normal plastic foam with micron-size cells. Sixty beams with direct-drive symmetry imploded the capsules. As predicted, the smaller pores gave a measurably higher yield.

In other experiments, the zero-order hydrodynamic motion of the two shells was measured using a unique implosion scheme. Forty OMEGA beams were pointed at calculated offset distances from the center—not at the center of the capsule. The other 20 beams created two 6.7-keV backlighter sources to radiograph the shell locations. The use of a sulfur-doped CH marker layer allowed measurement of the implosion with good contrast. Four goals were attained: First, the implosion hydrodynamics were measured by backlit imaging. Radiography from two simultaneous directions was used to image and measure the hydrodynamics of capsules that were optically thin to the x rays from the backlighters at 6.7 keV. Second, neutron yield and x-ray emission were used to measure the output from the thicker capsules with two different foam compositions to assess the effect of foam cell sizes on the implosion. The carbon resorcinol foam was found to increase the yield, as in the 60-beam shots, but the early results indicate little observable effect on the hydrodynamic behavior. Third, investigations were carried out to find out whether a thin layer of plastic overcoat would help separate the effect of absorption at the seam of the outer capsule from the seam hydrodynamics. However, the target quality was not good enough to allow the observation of a measurable difference. Fourth, the radius versus time of the sulfur marker layer was measured for the implosion of Au-coated and uncoated targets to determine the difference in the implosion due to the gold *M*-band x rays that exist in some of the NIF-design ICF capsules. The results were in good agreement with one-dimensional simulations (Fig. 100.86) although little difference was observed between the coated and uncoated targets.

Burn-History Diagnostic Development: In collaboration with LLNL, LANL continued to develop diagnostics that record the temporal behavior of the fusion burn. Gamma rays are a by-product of the deuterium–tritium (D-T) reaction. Using our two Gas Cerenkov Detectors (GCD's) (Fig. 100.87), these gamma rays are converted to relativistic electrons that emit Cerenkov radiation, which is then recorded. The prototype instrument, GCD1, records the emission using a photomultiplier tube and fast oscilloscope. The newer instrument, GCD2, records the information with higher time resolution using a streak camera.

During high-neutron-yield DT and deuterium–deuterium (DD) experiments conducted by LLE, both the GCD's and the LLE Neutron Temporal Detector were successfully operated simultaneously for the first time. Much cleaner and stronger signals were obtained with the streaked GCD2 (Fig. 100.88). These higher-quality signals allowed a GCD2 sweep rate of 10× for the gamma-burn signal. Quality GCD1 results were also obtained for most implosions.

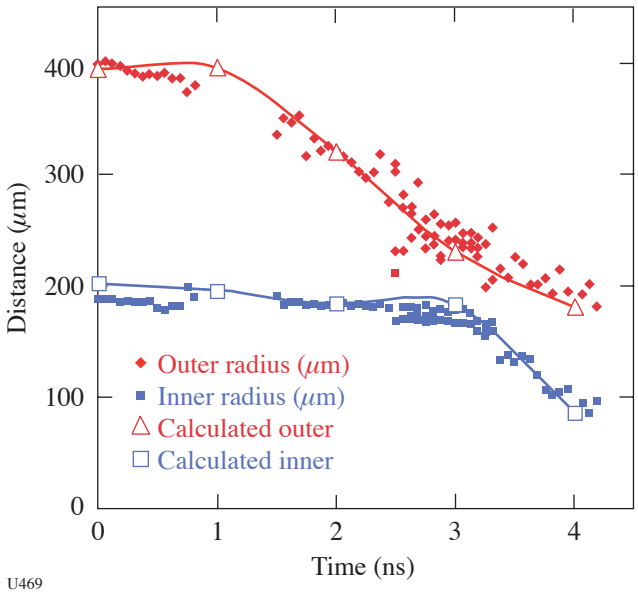

Figure 100.86
The temporal behavior of the outer and inner shells shows the momentum transfer between the two shells at about 3 ns. One-dimensional simulations are in good agreement with the measurements.

Figure 100.87
The GCD pressure cell and light-collecting optics are shown without the streak camera recording system.

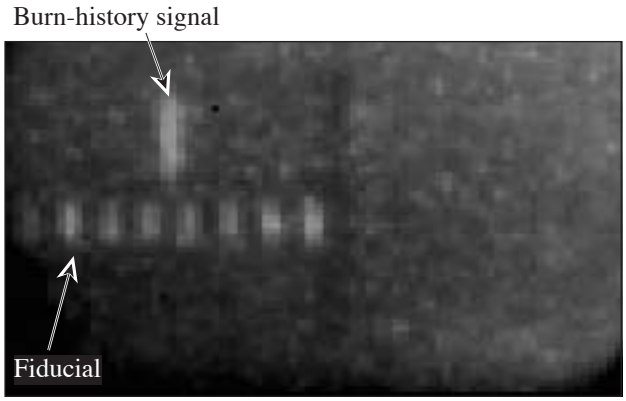

Figure 100.88
The time-resolved burn-history signal from a high-yield implosion demonstrated a 280-ps time resolution.

The feasibility of simultaneously recording a fusion gamma ray and fusion neutron signals using both the GCD1 *and* GCD2 was also successfully demonstrated; this simultaneous recording is an essential step in establishing the feasibility of a dual-mode capability in a single diagnostic. This recording was accomplished by placing either fused-silica glass or lead glass behind the normal converter foil and producing a *gas* Cerenkov signal and a *glass* Cerenkov signal on any given implosion. The neutron-burn signal was strong enough to allow a GCD2 sweep rate of 3×.

Beryllium Ablator Microstructure Stability (BAMS): An LANL goal is to deliver a specification for the microstructure of ignition-capsule ablators to the National ICF Program. The current focus is on beryllium–copper ablators, but other materials may be investigated as well.

LANL experiments make VISAR observations of ~1-Mbar shock waves in beryllium–copper samples, DANTE measurements of hohlraum temperature (verifying 6-ns-long composite pulses from OMEGA), x radiography of perturbations in samples, and characterization of the spectra from aluminum backlighters. In addition, LANL scientists also successfully recorded backlit ("side-lit") x radiographs of beryllium–copper samples viewed from the side, allowing a determination of the trajectory of the samples' motions. This permits one to make inferences about the radiation drive accelerating the samples, independent of the DANTE and VISAR data.

Another experimental series returned time-dependent data of the emission spectra of aluminum backlighters typical of those used in radiography of beryllium–copper samples. The relative contribution of line and continuum radiation was measured as a function of incident laser intensity to improve the contrast in our radiographs of intentionally perturbed samples and eventually in future radiographs of microstructure-perturbed samples.

Cylinder Implosion: Significant progress was made toward understanding the effect of convergence on shock-driven instability growth [Richtmyer–Meshkov (RM) instability] and initiated experiments that address variable acceleration (Rayleigh–Taylor) instability growth. Both types of instability can adversely affect ICF capsule implosions. High-quality data were also acquired on re-shock of already developing mix layers and defect–shell interactions. The primary effect of convergence on the single-mode RM instability is to postpone or suppress the growth of secondary instabilities resulting in an extended period of linear growth, well beyond that expected and observed in planar geometry.[2] The linear growth for several sinusoidal initial perturbations is shown in Fig. 100.89. Approximate linear growth is observed for amplitude-over-wavelength ratios as large as 4. The mechanism(s) responsible for the observed behavior has not been identified; however,

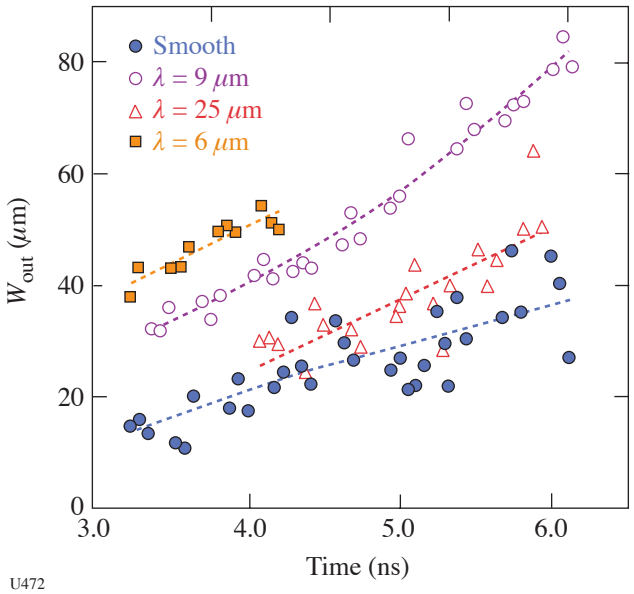

Figure 100.89
The growth of the mix layer width W_{out} for sinusoidal perturbations with an initial amplitude of 2 μm varies with the wavelength of the perturbations.

the apparent postponement of saturation is a dramatic example of the effect of convergence. To date, comparisons with computational (*RAGE*)[3] results have yielded qualitative agreement, but quantitative differences are still being addressed. The transition to turbulent mixing for short-wavelength ($\lambda \leq 2.5$-μm), multimode perturbations was also identified. Again, the apparent effect of convergence is to prolong linear growth for extended periods rather than the power-law-growth behavior observed in planar geometry. The short-wavelength results are being used to verify and validate the BHR model[4] in *RAGE* and to provide guidance in implementing crenulative (convergence) effects in the BHR turbulence model.

Off-Hugoniot Stability: The initial proof-of-principal experiments for the Off-Hugoniot Stability project were conducted this year. The goals of the integrated experiments were to evaluate whether radiography provides sufficient resolution of interface locations and to demonstrate that sufficient heating can be applied to generate hydrodynamic motion. The wedge experiments were designed to characterize the tin preheat source. Two experimental packages were employed: an integrated target [Figs. 100.90(a) and 100.90(b)] and a wedge target [Fig. 100.90(c)].

Both target types returned data that surpassed expectations. Five shots using integrated targets successfully captured the temporal expansion of the heated epoxy into the foam. Measurements were made at 2, 3, 4, 6, and 8 ns after the heating drive beams turned off. Figure 100.91(a) shows the epoxy layer at 3 ns with a final resolution between 15 and 20 μm, confirming that the experimental design provides sufficient measurement accuracy to meet the physics objectives of the campaign.

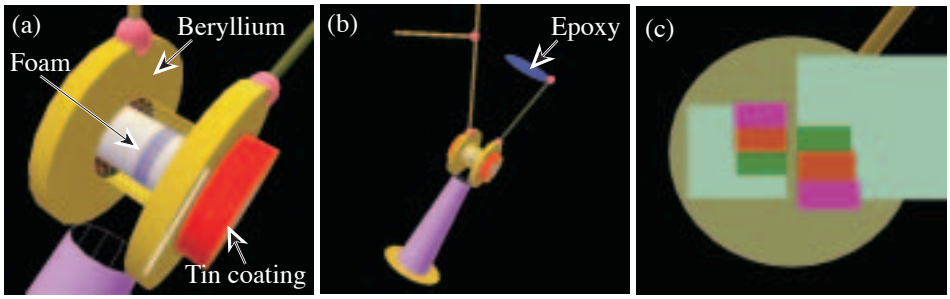

U473

Figure 100.90
(a) The integrated target consists of a beryllium assembly, stuffed with epoxy and foam layers. A thin coating of tin is directly driven by 33 beams to produce *L*-shell emission that heats the package. (b) The integrated target showing backlighter foil and view shield. (c) The wedge target measures the transmission of tin *L*-shell emission through wedges of epoxy and beryllium and facilitates an accurate measure of the *L*-shell–emitted flux.

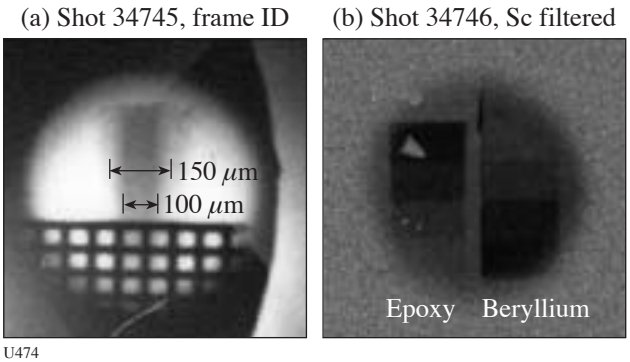

U474

Figure 100.91
(a) Radiograph of the epoxy layer 3 ns after the start of tin *L*-shell preheat. At this time, only 60% of the epoxy is still near full density. (b) The flat-field transmission of tin *L*-shell emission through the epoxy (left) and beryllium (right) wedges.

In addition to the success of the integrated experiments, the wedge targets along with extensive spectroscopic measurements were very effective at characterizing both the spectral nature and conversion efficiency of the tin *L*-shell emission. Figure 100.91(b) shows the tin *L*-shell transmission through characterized epoxy and beryllium wedges. These data suggest that about 2% to 5% of ultraviolet laser energy on target is converted to the tin *L* shell.

Astrophysical Jets: The jet project is a collaboration between LANL, AWE, and LLNL designed to verify and validate turbulence models for astrophysical simulations in our radiation-hydrodynamic codes. The jet target consists of a titanium foil mounted to a washer. A low-density, 0.12-g/cm^3, resorcinol-formaldehyde (RF) foam is mounted to the rear side of the titanium washer. The laser beams strike the titanium foil and drive a titanium jet into the foam. The primary diagnostic is x radiography of the titanium jet in the foam.

High-quality radiographs using new noise-mitigation techniques were obtained. These measurements included placing a 4-μm-thick CH coating on the drive side of the titanium foil. In addition, a large gold shield was mounted to the front of the target that prevented x rays from the coronal plasma created by irradiating the titanium foil from reaching the x-ray detector. The background problems of the past were reduced with a new "spot-backlighter" design of a small square (200 μm) of vanadium, surrounded by CH. The low-atomic-number (low-*Z*) plasma that is created by the backlighter laser beams helps contain the vanadium blowoff and reduces the spatial extent of the high-energy background. The backlighter images the target orthogonally to the direction of jet propagation.

The temporal evolution of the jet was captured at three different times. The result from one of these times, 400 ns after the laser drive, is shown in Fig. 100.92(a). There is a great level of detail in the image. For example, refractive effects are observed at the bow shock edge [Fig. 100.92(b)] and also mixing between the titanium and the RF foam is apparent in Fig. 100.92(c).

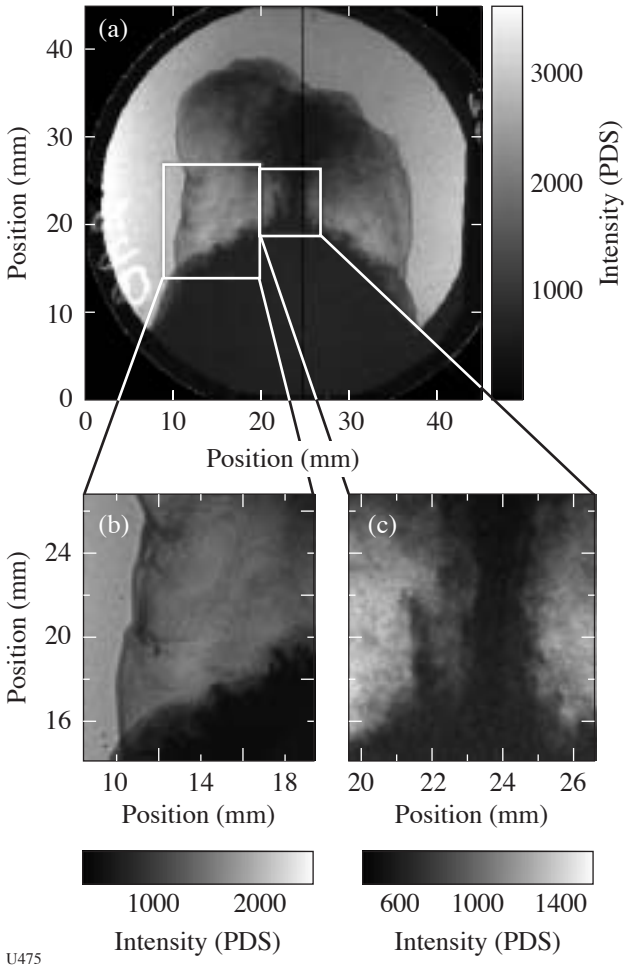

Figure 100.92
(a) Radiograph of the jet at 400 ns, magnified by a factor of 12. The jet stem is well collimated. The base (or pedestal) of the jet shows signs of hydrodynamic-instability growth. (b) Detail of the image showing the edge of the bow shock. Refractive enhancement of the bow shock is seen. (c) Detail of the jet stem showing the mixing between the titanium and the RF foam due to the Kelvin–Helmoltz instability.

Hohlraum Filling: Experiments on the NIF will use much more energy to heat a hohlraum of approximately the same size as an OMEGA hohlraum. An important constraint on the NIF experiments is how long the material will have to evolve before the hohlraum fills with gold from the wall of the hohlraum itself. A short series of experiments determined the amount of wall material influx in a hohlraum experiment and the effect of mitigation techniques on the radiation temperature achieved.[5]

It was found that coating the inner surface of the hohlraum with a 0.5-μm-thick layer of parylene would inhibit the amount of gold reaching the center of the hohlraum while decreasing the radiation temperature by only about 10 eV. Further experiments, however, showed that the number of hot electrons produced via laser–plasma interactions increased tremendously as measured by the level of hard x rays measured.

Backlighter Yield Measurements: The conversion efficiency of laser light into x-ray energy from titanium- and zinc-flat-disk targets was measured. These experiments were accomplished in half-day increments due to the simplicity of their configuration. Six drive beams illuminated the flat disks from one side using 1-ns square pulses. The number of beams and the focal-spot diameter were varied to produce orders-of-magnitude changes in the laser-irradiance conditions. Measurements were taken with framing cameras, streak cameras, and static pinhole cameras; however, the primary diagnostic was the Henway spectrometer [a time-integrated, x-ray-film–based survey spectrometer (Fig. 100.93)]. Every shot produced high-quality data that are currently being analyzed to determine the scaling of x-ray conversion efficiency as a function of laser irradiance. These results will be used to develop and refine area and point-backlighter configurations for OMEGA and future NIF experiments.

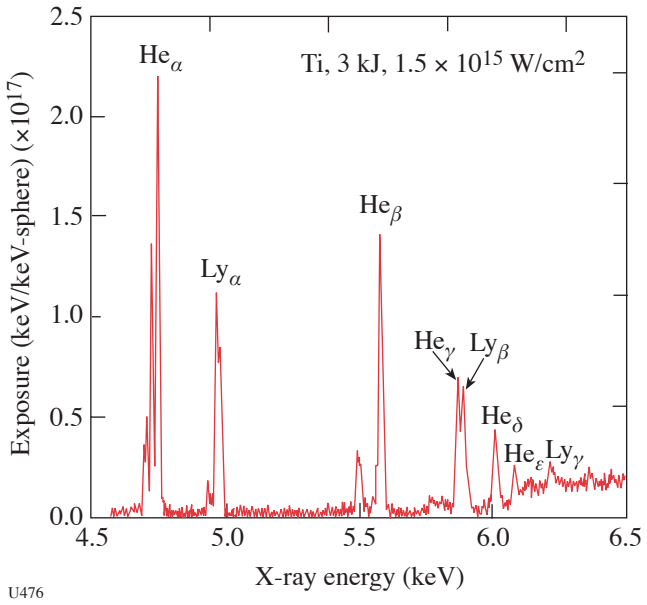

Figure 100.93
Example of data taken with the Henway spectrometer of the emission from a flat titanium target. Signals will be integrated over the helium-α emission line to determine conversion efficiency into bright line emission for future backlighter configurations.

FY04 SNL OMEGA PROGRAMS

SNL carried out 31 target shots on the OMEGA laser in FY04 and also participated in several of the campaigns led by other laboratories. The SNL-led campaigns included the following:

Modification of a Laser Hohlraum Spectrum via a Mid-Z Wall Liner: A typical laser hohlraum has a radiation spectrum that includes a significant component of non-Planckian, high-energy photons (such as Au *M*-band x rays) that originate in and near the hot, low-density coronal plasma in which the laser light is absorbed and converted into x rays. These hard x rays can have undesirable effects for an ICF application, such as causing preheat ahead of the shock front in the ablator of an indirect-drive capsule.[6] One concept for tailoring the spectrum in a hohlraum is to employ a thin, mid-*Z* liner to supply plasma for the x-ray conversion, with an underlying high-*Z* wall for x-ray containment. In a recent series of laser hohlraum experiments performed on OMEGA, this concept was demonstrated by employing a thin (0.5-μm) Cu liner on the interior of an Au-walled hohlraum to significantly soften the radiation spectrum and yet retain the peak hohlraum temperature of a standard Au hohlraum. As shown in Fig. 100.94(c) and 100.94(d), this successful result was evident in the data from the DANTE array of *K*- and *L*-edge filtered x-ray photocathodes.[7] A 280-nm Streaked Optical Pyrometer[8] was used to confirm that the preheat ahead of the shock front in a CH ablator was significantly reduced when using the Cu-lined hohlraum, as compared to an ordinary hohlraum [Fig. 100.94(b)].

The Effectiveness of Mid-Z Dopants in Reducing Preheat in Indirect-Drive ICF Ablator Materials: In previous work,[6,9] we experimentally verified that mid-*Z* dopants can be used to significantly reduce preheat and shock temperature in low-*Z*, indirect-drive ICF ablator materials. The previous experiments with Ge-doped CH ablators were done with dopant concentrations of 2% (atomic) Ge. As shown in Fig. 100.95, FY04 experiments have demonstrated that a significantly lower dopant concentration (0.5% atomic Ge in CH) can also be effective for reducing shock temperatures and preheat levels in indirect-drive ablators.

Long-Pulse Au Hohlraum Wall Albedo Measurements: In previous work,[10] measurements of absolute hohlraum wall albedos for ignition foot drive temperatures were made for pulse lengths of up to 1.5 ns. In FY04, we began work to extend the albedo measurements to longer pulse lengths and achieved albedo measurements for pulse lengths of ~3 ns. Two experimental arrangements were used in the long-pulse albedo experiments: a secondary hohlraum driven by x rays from a single primary hohlraum [Fig. 100.96(a)], and a secondary hohlraum driven by x rays from two primary hohlraums [Fig. 100.96(b)]. The secondary hohraum temperature history is shown in Fig. 100.97(a), and the new extension of the Au

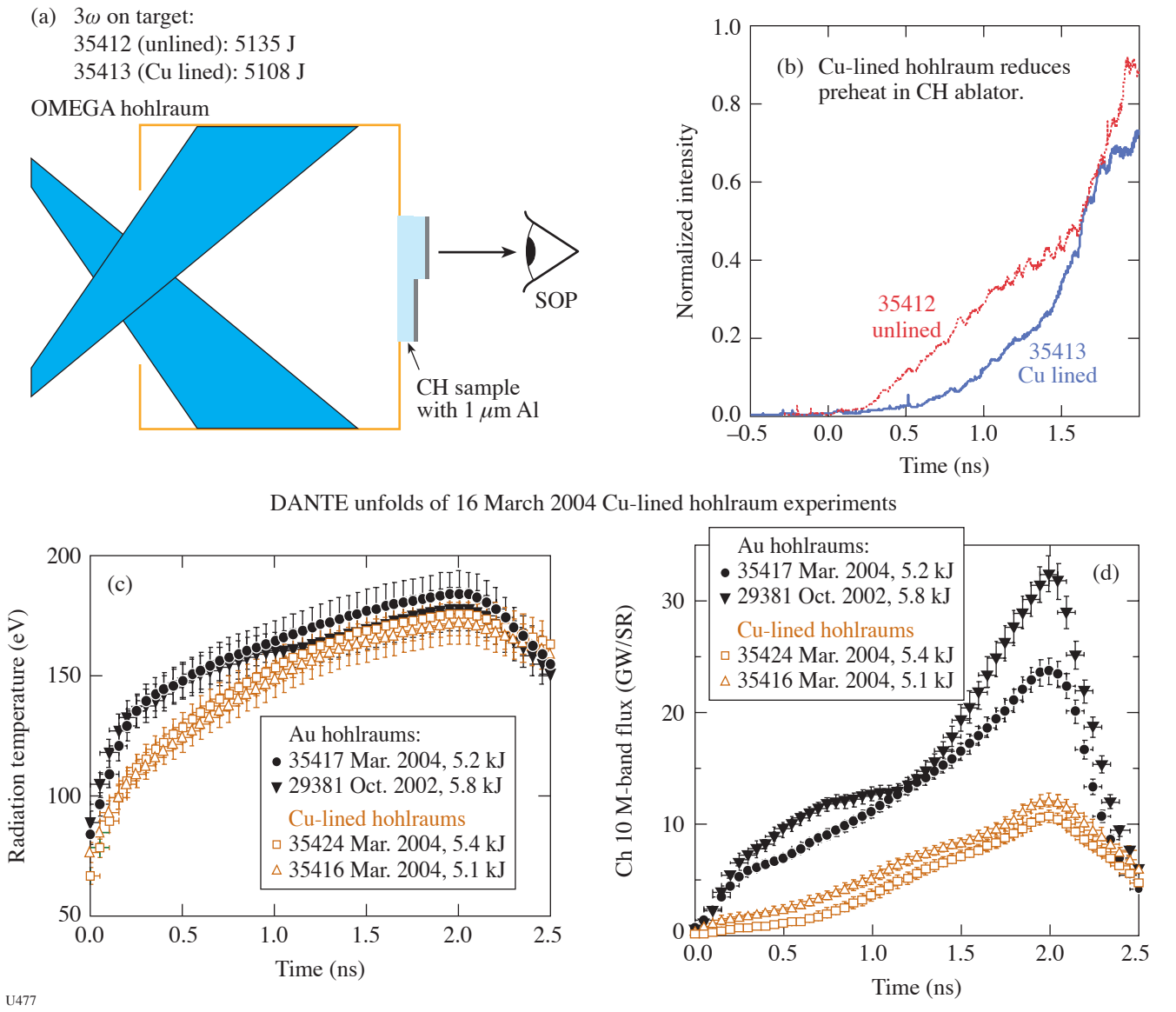

Figure 100.94
Results from experiments to demonstrate the modification of a laser hohlraum spectrum by using a mid-Z wall liner (Cu).

hohlraum wall albedo measurement is shown in Fig. 100.97(b).

Tests of a VISAR Time-Resolved Hohlraum Temperature Measurement Technique: In FY04, we began tests on a new technique for time-resolved hohlraum temperature measurement. The basic idea is to use VISAR[11] to track the velocity of a radiatively driven shock front in a quartz sample attached to the wall of a hohlraum. The experimental arrangement for the initial tests at OMEGA is depicted in Fig. 100.98. These initial tests utilized both DANTE and an aluminum step witness plate to confirm the drive temperature and were performed for hohlraum temperatures in the range of 110 to 190 eV. As shown in Fig. 100.99, the VISAR-measured shock velocity can be used to track the hohlraum temperature history. For the hohlraum radiation temperature range of these experiments, the empirical conversion $T_r = 21.7\, v_s^{0.57}$ has been used, where T_r is hohlraum temperature in eV and v_s is shock velocity in μm/ns. An important finding is that x-ray preheat presents a

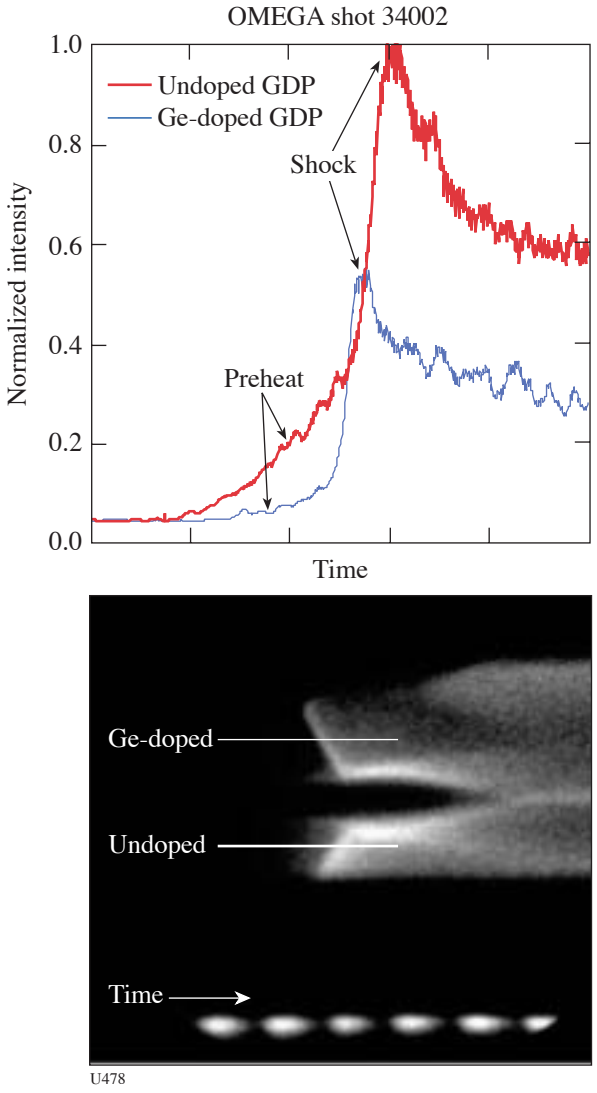

Figure 100.95
Results from experiments to demonstrate the effectiveness of mid-Z dopants to reduce preheat.

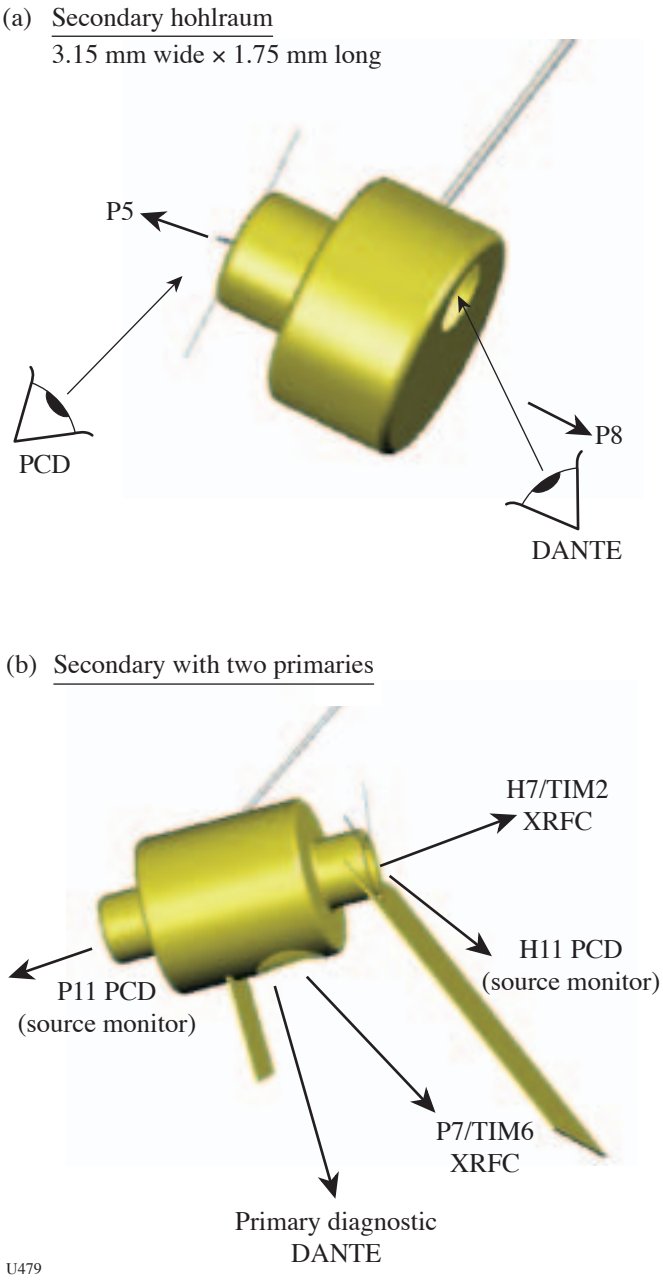

Figure 100.96
Schematic of long-pulse albedo experiments. (a) Secondary hohlraum driven with one primary hohlraum and (b) secondary hohlraum driven with two primary hohlraums.

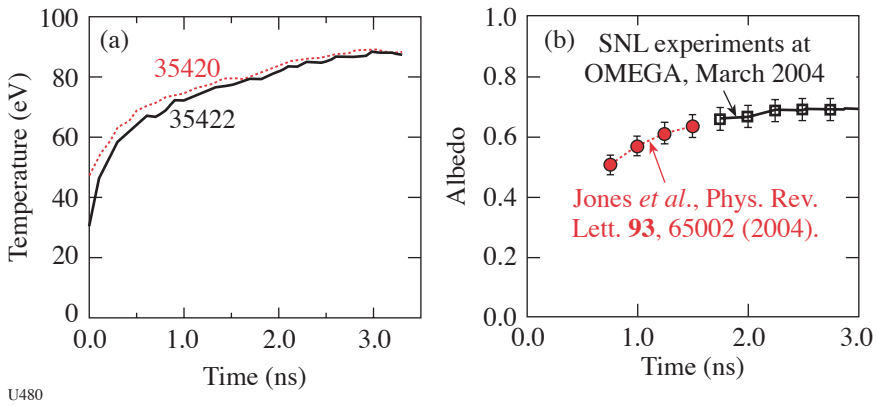

Figure 100.97
Temperature history of (a) secondary-hohlraum temperature and (b) albedo measurement.

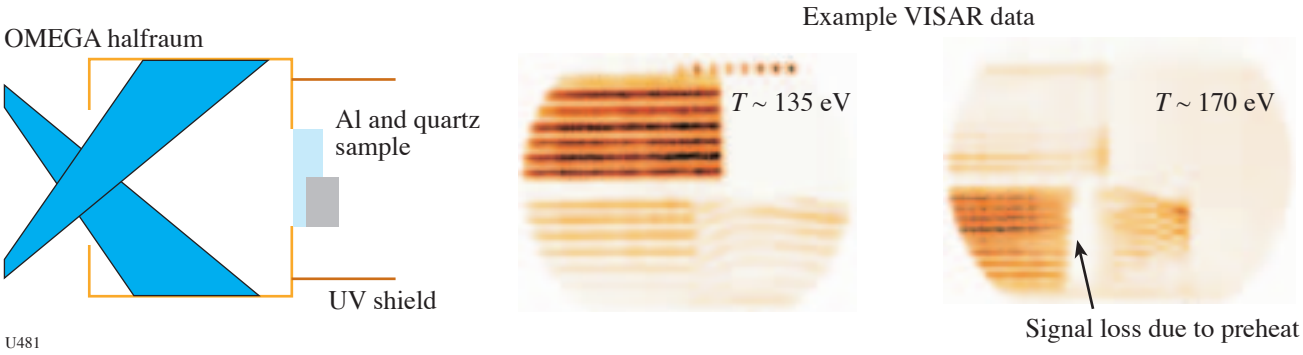

Figure 100.98
Experimental arrangement for SNL VISAR time-resolved hohlraum temperature measurement experiments.

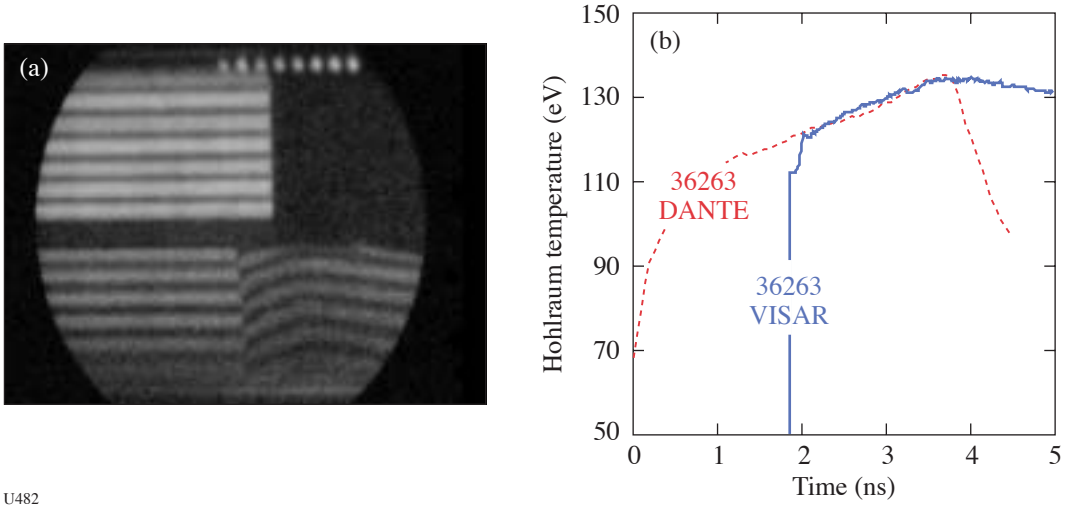

Figure 100.99
(a) VISAR velocity record and (b) resulting hohlraum temperature history from SNL experiment on OMEGA.

significant limitation to this technique for hohlraum temperatures above ~170 eV (as indicated in Fig. 100.98).

FY04 NRL Program Control of Laser Imprinting with High-Z Thin-Layer Targets

Principal Investigator: A. Mostovych

As part of a collaborative effort with NRL, a series of 13 OMEGA target shots were taken to investigate the control of laser imprinting.

The objectives of this experiment were to evaluate the impact of laser imprint under conditions similar to ICF-like reactor implosions and to test the effectiveness of controlling imprint from a high-power glass laser with the use of thin, high-Z-layer targets. In earlier work,[12] on the Nike KrF laser facility, it was demonstrated that thin, high-Z-layer targets are, in fact, very effective in mitigating imprint. It was not clear, however, if the differences between glass and KrF laser drivers, such as ASE, wavelength, or imprint details, are important and if the observed imprint mitigation had general validity irrespective of the laser driver.

In this work, the OMEGA laser was configured to drive a planar 30-μm CH target with multiple, full SSD beams. As is needed for high-gain target implosions, the target was accelerated on a low adiabat by compressing it with a single, low-intensity (10^{12} W/cm^2), early beam foot (~2 ns) and subsequently accelerating it with three to five full-intensity beams (~5×10^{13} W/cm^2). The residual laser nonuniformities that imprint the target in the compression phase are amplified by RT growth in the acceleration phase and are measured in the experiment by x-ray radiography. An example of the measured RT amplified imprint is shown in Fig. 100.100. If the same target is now coated with a thin layer of high-Z material (250 Å of gold in this work), the foot pulse quickly ablates this layer and creates a region of strong laser absorption that moves with the ablating gold away from the target surface. At the point of absorption, the gold becomes a strong soft-x-ray radiator and drives target ablation farther from a standoff distance of several hundred microns. The separation of the absorption and ablation regions leads to a strong reduction in pressure nonuniformities on the target surface, thus mitigating the role of laser imprint. An example of this reduction is displayed in Fig. 100.101. Initial measurements of the Rayleigh–Taylor instability amplified imprint are displayed for targets with and without the thin gold layer. A clear reduction for the layered targets is observed. These results are in agreement with the initial Nike measurements but do not show as large of an effect. This is expected because thinner gold layers had to be used to compensate for the shorter foot and thinner targets that could be deployed on the OMEGA facility. The initial results indicate that the control of imprint with high-Z-layer targets is a robust effect, not sensitive to the type of laser driver. It is expected that

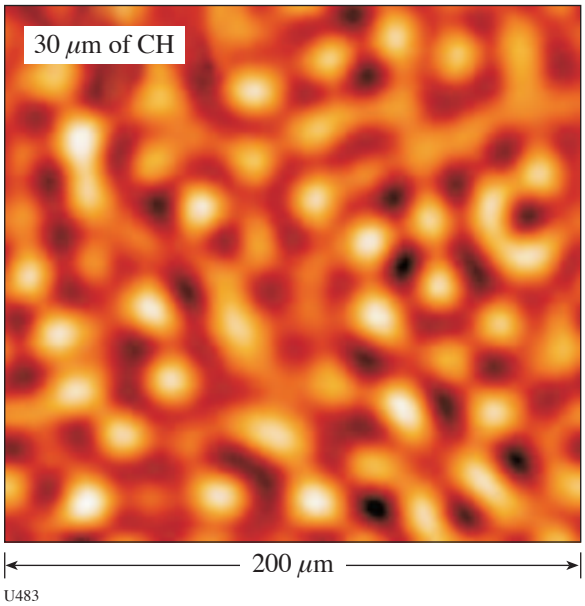

Figure 100.100
Typical mass nonuniformity of Rayleigh–Taylor amplified laser imprint at 3 ns into the main acceleration phase of a planar CH target.

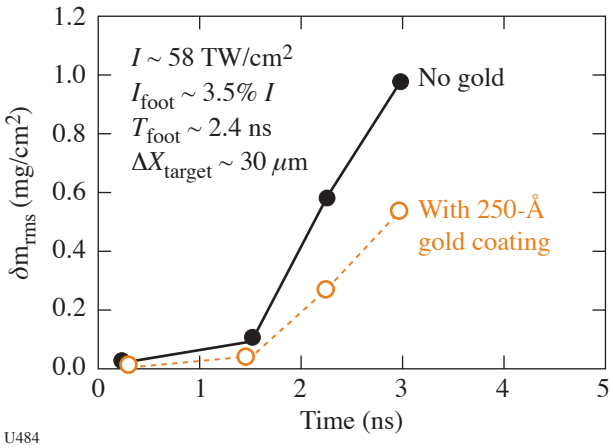

Figure 100.101
Comparison of amplified imprint with and without a thin gold coating on the ablation surface of the target. The thin, high-Z layer has a pronounced effect in reducing the level of imprint by almost 50%.

future near-term experiments will investigate the role of such high-Z layers in spherical implosions.

FY04 CEA Program

A total of 32 target shots led by CEA (Commissariat à l'Énergie Atomique, France) were carried out on OMEGA in FY04. The corresponding four experimental campaigns studied (a) laser–plasma interaction (LPI) in long-scale-length plasmas relevant to NIF/LMJ indirect-drive conditions; (b) irradiation symmetry and x-ray conversion efficiency in empty gold hohlraums; (c) production and optimization of multi-keV x-ray sources (performed on LLNL-owned shots); and (d) hydrodynamic instabilities in planar geometry. A summary of the LPI campaign is given in this section. The CEA diagnostics team also pursues a strong activity in the area of neutron detectors and neutron-induced effects on MJ-class laser detectors in collaboration with LLE teams. LLE direct-drive implosions provide a valuable neutron source for testing new concepts in this field.

The Thomson-scattering configuration for probing electron-plasma waves stimulated by the Raman backscattering instability (SRS) tested on OMEGA in FY03 was used in FY04 to study the SRS growth and saturation in gas-bag plasmas. As a first step, space-resolved measurements of SRS activity were performed along the interaction-beam propagation axis (z). This is achieved by pointing the probe beam at different locations along the z axis (see Fig. 100.102). With a series of five shots, we have been able to assess the SRS growth along the z axis (see Fig. 100.103). These space-resolved measurements evidence a completely different spatial SRS growth depending on the time during the interaction pulse. At early time, when the heaters are on, the SRS activity is saturated with a constant level observed over more than 1 mm. Toward the end of the interaction pulse, the SRS activity peaks sharply near the input side of the interaction beam as expected from linear convective amplification theory.

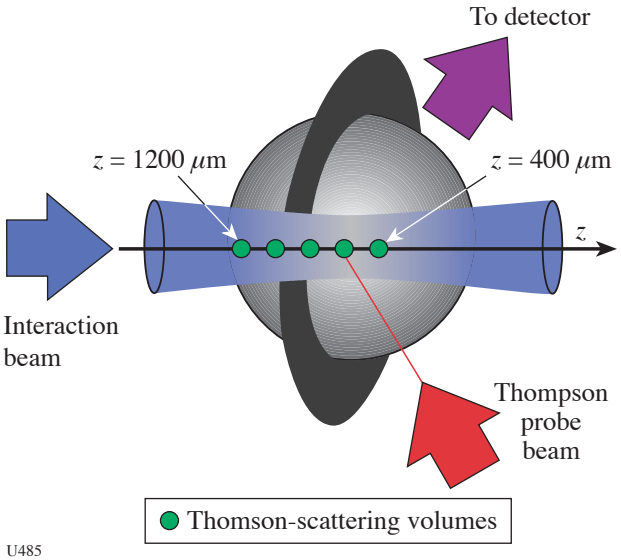

Figure 100.102
Schematic showing experimental configuration and the different probe-pointing locations of gas-bag targets.

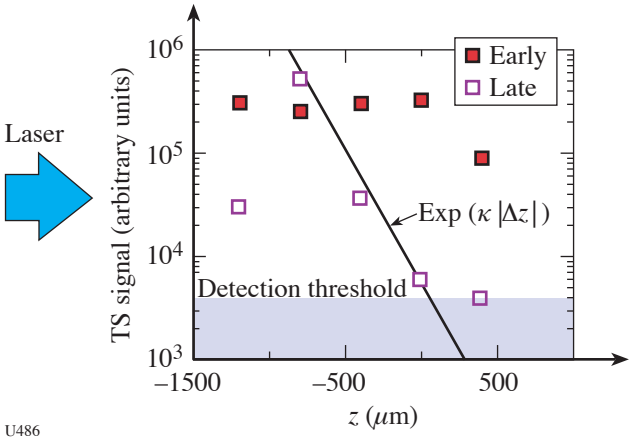

Figure 100.103
Thomson-scattering signals as a function of z in the early (t = 0.6 to 1.1 ns, when the heaters are on) and late (t = 1.2 to 1.7 ns) time periods. The exponential fit of the late time measurements gives a spatial growth rate of $\kappa = 6 \times 10^{-3}$ μm^{-1}.

REFERENCES

1. P. Loubeyre *et al.*, High Press. Res. **24**, 25 (2004).
2. J. R. Fincke *et al.*, Phys. Rev. Lett. **93**, 115003 (2004).
3. R. M. Baltrusaitis *et al.*, Phys. Fluids **8**, 2471 (1996).
4. D. Besnard, F. H. Harlow, and R. Rauenzahn, Los Alamos National Laboratory, Los Alamos, NM, Report LA-10911-MS (1987).
5. S. H. Batha and J. R. Fincke, "Quantified Reduction of Wall Material Influx During Hohlraum Experiments," to be published in the Review of Scientific Instruments.

6. R. E. Olson *et al.*, Phys. Rev. Lett. **91**, 235002 (2003).

7. H. N. Kornblum, R. L. Kauffman, and J. A. Smith, Rev. Sci. Instrum. **57**, 2179 (1986).

8. J. A. Oertel *et al.*, Rev. Sci. Instrum. **70**, 803 (1999).

9. R. E. Olson, R. J. Leeper, A. Nobile, J. A. Oertel, G. A. Chandler, K. Cochrane, S. C. Dropinski, S. Evans, S. W. Haan, J. L. Kaae, J. P. Knauer, K. Lash, L. P. Mix, A. Nikroo, G. A. Rochau, G. Rivera, C. Russell, D. Schroen, R. J. Sebring, D. L. Tanner, R. E. Turner, and R. J. Wallace, Phys. Plasmas **11**, 2778 (2003).

10. O. S. Jones *et al.*, Phys. Rev. Lett. **93**, 065002 (2004).

11. L. M. Barker and R. E. Hollenbach, J. Appl. Phys. **43**, 4669 (1972).

12. S. P. Obenschain *et al.*, Phys. Plasmas **9**, 2234 (2002).